Research Project on CO_2 Geological Storage and Groundwater Resources

Large-Scale Hydrological Evaluation and Modeling of the Impact on Groundwater Systems

Annual Report: October 1, 2006 to September 30, 2007

Contact: Jens Birkholzer
Earth Sciences Division, Lawrence Berkeley National Laboratory
1 Cyclotron Rd., MS 90-1116; 510-486-7134; jtbirkholzer@lbl.gov

Contributors: Jens Birkholzer, Quanlin Zhou, Jonny Rutqvist, Preston Jordan, Keni Zhang, Chin-Fu Tsang

NETL Program Manager: William O'Dowd

Executive Summary

If carbon dioxide capture and storage (CCS) technologies are implemented on a large scale, the amounts of CO_2 injected and sequestered underground could be extremely large. The stored CO_2 then replaces large volumes of native brine, which can cause considerable pressure perturbation and brine migration in the deep saline formations. If hydraulically communicating, either directly via updipping formations or through interlayer pathways such as faults or imperfect seals, these perturbations may impact shallow groundwater or even surface water resources used for domestic or commercial water supply. Possible environmental concerns include changes in pressure and water table, changes in discharge and recharge zones, as well as changes in water quality. In compartmentalized formations, issues related to large-scale pressure buildup and brine displacement may also cause storage capacity problems, because significant pressure buildup can be produced. To address these issues, a three-year research project was initiated in October 2006, the first part of which is summarized in this annual report.

Through numerical modeling of idealized subsurface formations, we have evaluated the possible impact of CO_2 injection on regional multilayered groundwater systems. To date, systematic modeling studies have been conducted for two basic CO_2 storage scenarios. For compartmentalized multilayer formations with closed lateral boundaries, we have evaluated the pressure buildup and storage capacity in response to CO_2 injection, via numerical simulations as well as approximate solutions. For laterally open multilayer formations, we have simulated the pressure buildup and brine migration patterns, and have analyzed their respective regions of influence. Several key conclusions can be drawn as follows:

<u>Compartmentalized Formations:</u>

1) The available volume for CO_2 storage in closed/semi-closed systems is mostly provided by pore compressibility and brine compressibility in response to formation pressure buildup, as well as leakage of native brine into and through seals, depending on the seal properties.
2) The storage capacity in compartmentalized system with impervious seals is found to be generally much smaller than in open systems, because geomechanical damage due to overpressure needs to be avoided. A maximum efficiency factor of about 0.005 was estimated for typical sandstone properties and the hydrologic conditions studied in this report, with similar storage contributions provided by pore and brine compressibility. In other words, only 0.5% of the initial pore volume would be available for storage of CO_2.
3) Only formation-seal systems with very small seal permeability of 10^{-20} m^2 or less exhibit a true closed-system behavior; i.e., only then is the displacement of native brine into and through the bounding seals so small that the pressure buildup is similar to a closed system. With seal permeability varying from 10^{-19} m^2 to 10^{-17} m^2, brine leakage had a moderate to strong effect in reducing or limiting the pressure buildup in the storage formation, thus allowing for considerably higher storage efficiency than a true closed system (while CO_2 was still safely trapped because of the combined capillary and permeability barriers).

Laterally Open Formations:

1) The region of influence in response to CO_2 injection can be extremely large. For the radial-symmetric domain evaluated in this study, considerable pressure buildup was observed 100 km away from the injection zone (up to one bar for certain sensitivity cases). Such pressure changes may cause problems if experienced in near-surface groundwater systems, a possible concern for a storage formation that extends updip to form a freshwater resource. If such environmental concerns prove to be important at a given site, the potential CO_2 storage capacity of a storage formation may be strongly reduced.

2) While the pressure pulse travels fast and far in saturated subsurface formations, the lateral brine flow velocities are found to be quite small, not much larger than those of natural groundwater flows in deep basins. The migration distance of a particle dissolved in the native brine (at a location a few miles away from the eventual CO_2 plume) is only a few hundred meters or less for a time period of 100 years during and after injection. We caution that these results have been obtained for a radial-symmetric system assuming a single-source injection site.

3) Characteristics of pressure buildup and brine displacement are not only sensitive to the key properties of the storage formation (e.g., lateral permeability, pore compressibility), but also strongly affected by the properties of the multilayered sandstone/shale sequence overlying and underlying the storage formation. Seals that are suitable for long-term trapping of CO_2 may allow for considerable brine leakage out of the formation vertically upward and downward. As a result, the pressure buildup and lateral flow in the storage formation is moderately to strongly reduced compared to a perfect seal with zero or close-to-zero permeability.

Our results demonstrate clearly the importance of evaluating the hydrologic perturbations generated by CO_2 storage. Any site assessment should consider the constraints imposed by pressure perturbation and brine displacement, either to avoid shallow-water impacts in open systems or to account for pressure constraints in closed systems. When investigating these issues, it is important to consider not just the storage formation, but also the multilayer characteristics of the site. While the key properties of multilayered groundwater systems have been varied in a sensitivity study, which has enabled us to draw the above general conclusions, certain model simplifications and parameter choices may be inadequate at given storage sites. Thus, the systematic simulations conducted here should lead into site-specific modeling of CO_2 storage candidate sites, representing the local hydrogeological conditions. Two site-specific modeling studies of likely candidate sites for CO_2 storage, probably in the Illinois Basin and the California Central Valley, will be conducted in a future project phase.

Table of Contents

List of Figures

List of Tables

1. Motivation

If carbon dioxide capture and storage (CCS) technologies are implemented on a large scale, the amounts of CO_2 injected and sequestered underground will be extremely large. Various research studies have been conducted to date evaluating under which hydrogeological conditions the injected volumes of CO_2 can be safely stored over hundreds or even thousands of years. For example, many of these studies address issues such as the long-term efficiency of structural trapping of CO_2 under sealing layers or the importance of other trapping mechanisms such as dissolution of CO_2 into formation water or mineral trapping as CO_2 reacts with the rock. Less emphasis has been placed on the understanding of the fate of the native brines or brackish waters that are being displaced by the injected volumes of CO_2. As discussed below, large-scale injection of CO_2 impacts subsurface volumes much larger than the CO_2 plume. Thus even if the injected CO_2 itself is safely trapped in suitable geological structures, large-scale injection and related brine displacement may affect shallow groundwater resources. The issue of brine displacement, and its possible environmental impact on groundwater hydrology, is addressed in the research effort reported here.

Figure 1 shows schematically the large-scale subsurface impacts that will be experienced during and after industrial-scale injection of CO_2. While the CO_2 plume at depth may be safely trapped under a low-permeability caprock with anticlinal structure, the footprint area of the plume is smaller than the footprint area of the displaced brine, which in turn is much smaller than the footprint area of elevated pressure. The footprint area of displaced brine illustrates the approximate location of a displaced fluid volume that was originally located within the CO_2 plume footprint. Of course, brine displacement occurs, to some degree, wherever a pressure gradient develops in response to injection, suggesting the possibility of water quality changes as brines or brackish water may migrate into freshwater regions. The footprint area of elevated pressure indicates the extremely large subsurface volumes where such pressure impacts might be expected.

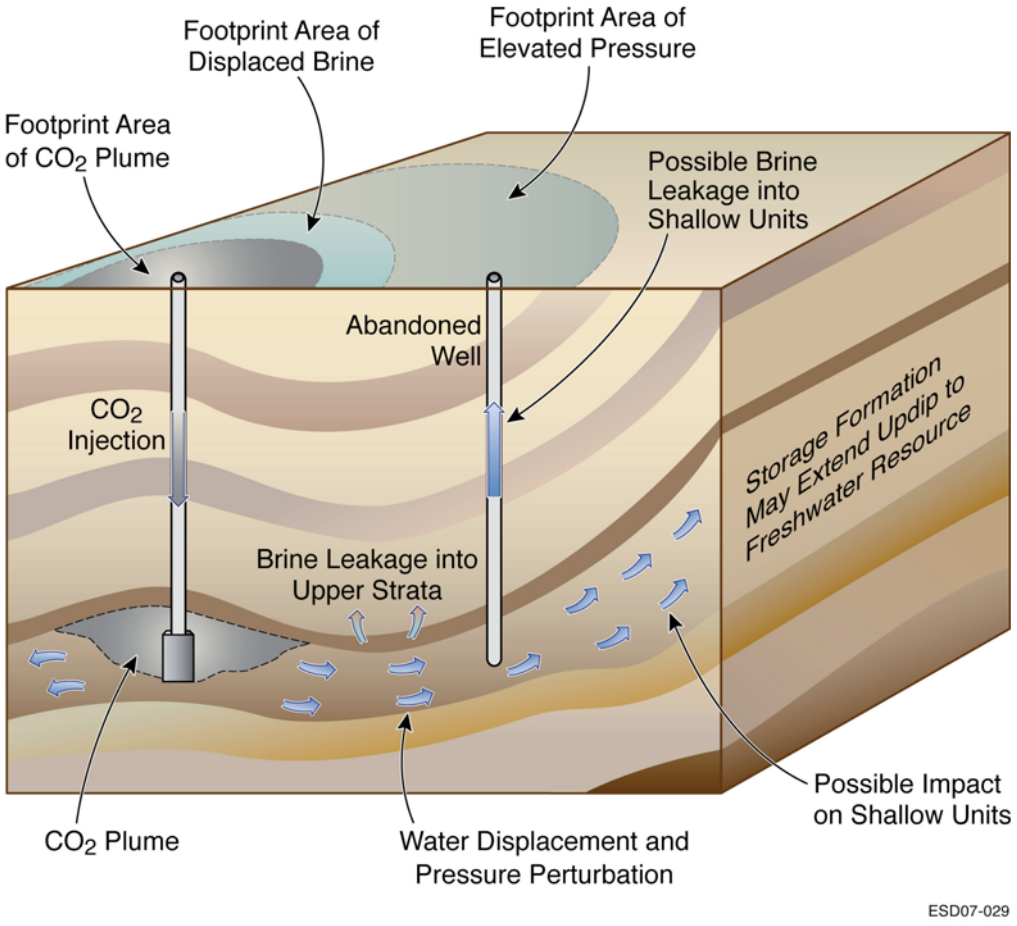

Figure 1. Schematic showing different regions of influence related to CO_2 storage

The environmental impact of large-scale brine displacement depends to a large extent on the hydraulic connectivity between deep storage formations and the freshwater aquifers overlying them. One primary concern would be a storage formation that extends updip to form a freshwater resource used for domestic or commercial water supply. Via this direct hydraulic communication, CO_2 storage at depth will impact the shallow portions of the aquifer, which could experience pressure increase and water table rise, changes in discharge and recharge zones, and changes in water quality. Even if separated from deep storage formations by sequences of low-permeability seals, freshwater resources may be hydraulically communicating with deeper layers, and the pressure buildup at depth would then provide a driving force for upward brine migration. This can be, for example, via local high-permeability flow paths such as faults and abandoned boreholes. In addition,

seals may pinch out or have higher permeabilities locally allowing for vertical inter-layer migration. Finally, land surface deformation or uplift is expected in response to CO_2 injection, which may change surface and near-subsurface flow patterns even without a hydraulic direct impact of brine displacement. The reverse effect, land subsidence in response to groundwater withdrawal (e.g., for water supply, agriculture, or related to oil production), is a common problem throughout the United States (USGS, 1999).

Issues related to large-scale pressure buildup and brine displacement may also cause operational and capacity problems. For example, if more than one large point source was to store CO_2 into the same formation, the operational scheme and the location of the injection zone would have to be carefully planned as to avoid unwanted feedback between neighboring sites. Storage capacity may be a concern in compartmentalized formations, as depicted in Figure 2, from which the displaced CO_2 can not easily escape laterally to make room for the injected CO_2 (closed systems). When large volumes of CO_2 are injected into a closed system, a significant pressure buildup will be produced, which can severely limit CO_2 storage capacity, because overpressure and geomechanical damage need to be avoided (Rutqvist and Tsang, 2002; Rutqvist et al., 2007a, 2007b).

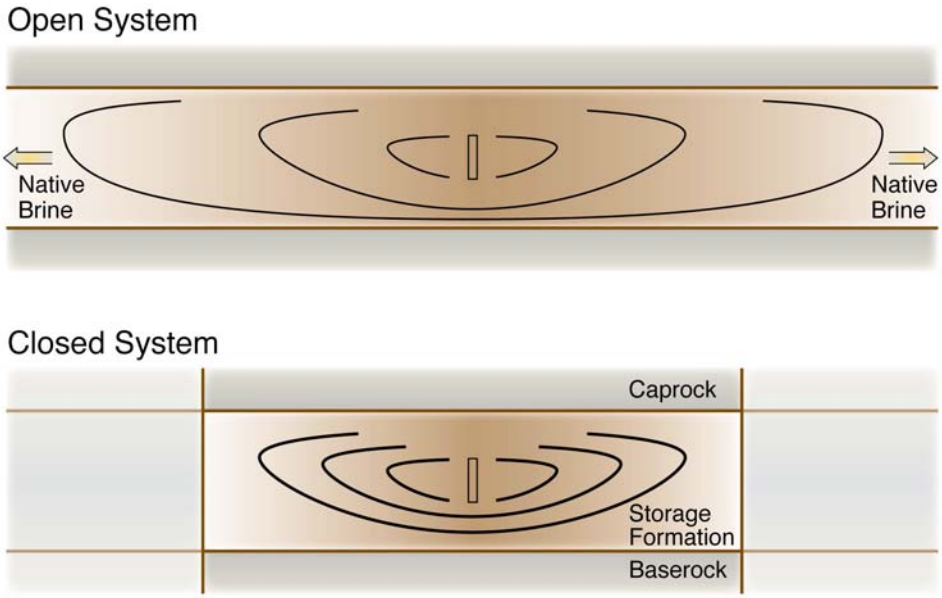

Figure 2. Schematic showing open systems versus closed systems (not to scale)

The above considerations suggest that evaluation of site suitability with respect to volumetric capacity as well as environmental impact should include (1) a study on the expected pressure buildup and brine displacement, and its impact on the shallow subsurface, and (2) a site characterization effort that includes the large region of influence dictated by subsurface pressure changes.

2. Research Scope

To date, the impact of large-scale CO_2 injection and related brine displacement on regional multilayered groundwater systems has not been systematically assessed. To build confidence in carbon capture and storage technologies, there needs to be an adequate understanding of the magnitude and extent of water pressure increase in the storage formation and in the shallower aquifers, which may be separated by aquitards of much smaller hydraulic conductivities. In particular, the change in groundwater table level, the effect on discharge and recharge zones in the groundwater system, and the impact of these changes on the properties and characteristics of underground sources of drinking water (USDWs) should be investigated. Estimates of CO_2 storage capacity should consider constraints imposed by brine displacement, either to avoid shallow-water impacts in open systems or to account for pressure constraints in closed systems. To address these research needs, the following research project was initiated in 2006, the first part of which is described in this annual report. The following tasks included in the research program have a successive degree of complexity, starting with systematic studies of idealized formations leading up to detailed modeling studies of one or two groundwater basins in the U.S. that are likely candidates for future storage of CO_2.

Task 1: Storage Capacity and Pressure Buildup in Idealized Pressure-Constrained Storage Formations (Closed Systems)

Analytical and numerical solutions are employed that allow a fast evaluation of brine displacement by injected CO_2 and the related pressure buildup in simplified geological systems such as shown in Figure 2 (bottom). The objectives are to:

- Develop a basic understanding of potential pressure buildup in closed systems
- Determine sensitivity of pressure buildup and storage capacity to injected volume, formation size, hydraulic properties, compressibility, and other key parameters
- Develop a quick assessment method for estimating storage capacity in pressure-constrained formations

Task 2: Pressure Buildup and Brine Displacement in Idealized Multilayered Groundwater Systems (Open Systems)

A semi-analytical or numerical simulation study is conducted to evaluate the brine displacement by injected CO_2 and the related pressure buildup in a multilayer geological system. The objectives are to:

- Develop a basic understanding of the potential pressure buildup (in lateral and vertical direction) in a laterally open storage formation such as shown in Figure 2 (top)
- Explore the effects of interlayer communication through low-permeability seals
- Explore the effects of interlayer communication through faults, fracture zones, or wells
- Evaluate the impact on groundwater table rises, discharge-recharge zones, and water quality changes in the shallower groundwater layers, including USDWs

Task 3: Hydromechanical Aspects of Injection in Idealized Multilayered Groundwater Systems

This task is an extension of previous tasks to account for hydromechanical effects that could potentially impact the expected pressure buildup and multilayer interaction. The objectives are to:

- Evaluate the role of mechanical deformation, with associated permeability changes, on pressure buildup, water displacement, and land surface uplift, etc.
- Evaluate hydrogeological and mechanical effects in shallower units and USDWs

Task 4: Analysis and Modeling of One or Two Regional Groundwater Systems

This task involves modeling evaluation of one or two regional groundwater systems in response to CO_2 injection. Two deep saline aquifer systems have been chosen based on the interaction with regional partnerships. The objective is to evaluate pressure buildup and brine displacement for these real-world examples.

The following Sections 3 and 4 of this report document the progress made during the first project year, with respect to Tasks 1 and 2, respectively. Tasks 3 and 4 have not yet started, but preparatory work has been conducted, as reported in Section 5.

3. Idealized Pressure-Constrained Storage Formations

The storage capacity and transient pressure buildup in response to industrial-scale CO_2 injection into a compartmentalized saline formation is evaluated using detailed numerical simulations with the TOUGH2/ECO2N simulator (Pruess et al., 1999; Pruess, 2005). Our focus here is to understand the reservoir conditions as a function of various reservoir parameters. In addition, we have developed simple analytical (quick-assessment) expressions that provide estimates for the storage capacity and pressure buildup in such pressure-constrained systems. Results from the numerical simulations are compared with those estimated through the quick-assessment method for various sensitivity cases. The good agreement indicates that the analytical method produces reasonable estimates for compartmentalized storage formations.

3.1. Background

In certain geological situations, a storage site targeted for CO2 sequestration may be a compartmentalized reservoir laterally separated by low-permeability zones. These zones may be formed by natural heterogeneity and/or faulting. When such a reservoir, bounded vertically by impervious seals, is surrounded on all sides by barriers of very low permeability, this reservoir acts as a “closed” system (Figure 3, top). Evidence of such closed systems has been found in hydrocarbon reservoirs, as indicated by sharp changes in fluid pressure along the reservoir boundaries (Neuzil, 1995; Puckette and Al-Shaieb, 2003; Muggeridge et al., 2004). When large volumes of CO_2 are injected into a closed system, a significant pressure buildup will be produced. This pressure buildup can severely limit the CO_2 storage capacity, because overpressure and geomechanical damage need to be avoided (Rutqvist and Tsang, 2002; Rutqvist et al., 2007a, 2007b). In this case, the storage capacity mainly depends on pore and brine compressibilities that provide expanded pore space available for storing the injected CO_2, and on the maximum pressure buildup that the formation can sustain.

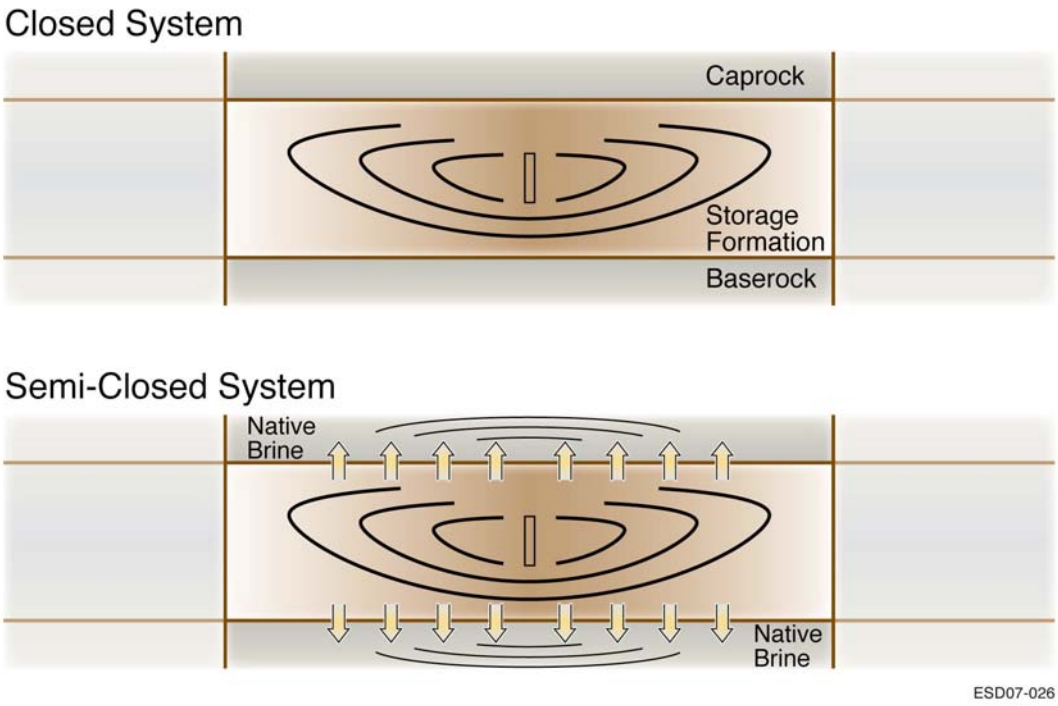

Figure 3. Schematic showing closed and semi-closed systems (not to scale)

Of course, the overlying and underlying seals of a storage aquifer are not perfectly impervious, allowing the pressure buildup caused by CO_2 injection and storage to partially dissipate into and through these seals. In this case, the saline aquifer acts like a "semi-closed" system (Figure 3, bottom), allowing some fraction of the displaced brine to migrate into and through the overlying and underlying sealing units, which in turn would increase the storage capacity for CO_2. The importance of this vertical inter-layer communication will mostly depend on the permeability of the seals, which can vary widely depending on their hydrogeological characteristics (e.g., Neuzil, 1994; Domenico and Schwartz, 1998; Hovorka et al., 2001; Hart et al., 2006). Relatively permeable sealing units (e.g., with permeability on the order of 10^{-18} m^2) may allow considerable vertical leakage of brine out of the storage aquifer, in which case pressure buildup may be reduced, and pressure constraints may not be a limiting factor in CO_2 storage capacity.

To our knowledge, no research has been conducted to date to estimate the transient pressure buildup and CO_2 storage capacity in pressure-constrained systems. Our research

therefore aims at (1) developing a basic understanding of potential pressure buildup in compartmentalized systems, (2) determining sensitivity of pressure buildup and storage capacity to injected volume, formation size, hydraulic properties, compressibility, and other key parameters, and (3) developing and applying a quick assessment method for estimating storage capacity in deep closed and semi-closed saline formations, complementing existing methods for capacity estimates in open systems (DOE, 2007).

The quick-assessment method is based on the fact that the injected CO_2 needs to displace native brine of an equivalent volume, and that this equivalent volume is comprised of three volume contributions that can be easily calculated: (1) the additional pore volume within the storage formation provided by pore and brine compressibility in response to pressure buildup; (2) the additional pore volume within the sealing units provided by pore and brine compressibility in response to pressure buildup; and (3) the leakage of the displaced brine through the seals into overlying/underlying formations. The validity of the method is demonstrated by comparing the estimated storage capacities to the "true" values calculated through detailed modeling of multiphase flow and multicomponent transport of CO_2 and brine. The validity range is demonstrated for a range of hypothetical formation-seal systems, with varying lateral radial extent (i.e., pore volume) and hydrogeologic properties (i.e., permeability).

With these goals in mind, this section is structured as follows: Section 3.2 introduces the hypothetical formation-seal systems analyzed and discusses the different sensitivity cases with varying geometric and hydrogeologic properties; Section 3.3 describes the quick-assessment method for estimating the pressure buildup and storage capacity in closed and semi-closed systems; Section 3.4 gives simulated results showing the observed pressure buildup and CO_2 plume evolution for a range of conditions; and Section 3.5 demonstrates the applicability and validity of the quick-assessment method through comparison against the simulated results.

3.2. Numerical Simulations

To obtain the "true" CO_2 storage capacity of pressure-constrained formations, we developed a numerical model simulating the multiphase flow and multicomponent transport of CO_2 and brine in a hypothetical deep saline formation, using the TOUGH2/ECO2N simulator (Pruess et al., 1999; Pruess, 2005). The transient pressure buildup and detailed spatial CO_2 plume evolution were simulated for closed systems with impervious seals and for semi-closed systems with non-ideal seals. We conducted different simulation runs, varying radial extent to evaluate the effect of the lateral boundary condition (storage formation size), varying formation permeability to evaluate the propagation of pressure buildup and related sensitivities, and varying seal permeability to investigate the effect of brine leakage into and through the seals and its impact on storage capacity.

For each simulation run, we calculated a storage efficiency factor, *E*, defined as the fraction of stored volume of CO_2, V_{CO2}, per initial total pore volume of the storage formation, V_F. This is the same definition used in the capacity estimates for open systems described in DOE (2007). If the simulated pressure buildup in the storage formation at the end of the injection period is less then a previously defined sustainable pressure buildup (Section 3.3.5), the designated storage scenario is not pressure-constrained, and we refer to *E* as the *actual storage efficiency*. In contrast, in cases where the simulated pressure buildup is close to or exceeds the sustainable pressure buildup (which may occur before reaching the designated injection volume), the storage scenario is pressure-constrained. In such cases, we refer to *E* as the *maximum storage efficiency*. Through our detailed numerical simulations, the storage capacity estimates account for CO_2 stored in its own supercritical phase as well as the smaller amount of CO_2 dissolved in brine. The simulation results also consider all details related to the non-uniform pressure buildup and CO_2 plume evolution, thus obtaining the "true" CO_2 storage conditions.

3.2.1. Model Setup

A two-dimensional radially symmetric model domain was chosen representing a deep saline aquifer. The storage formation, located at a depth of approximately 1,200 m (top of formation) below the ground surface, is 250 m thick and bounded at the top and bottom by sealing units (caprock and baserock) of 60 m thickness each (see Figure 4). The outer lateral boundary has a no-flow condition; i.e., brine is not allowed to escape from the model domain. In the base case, the model domain has a radial extent of 20 km, and the sealing units are assumed to be impervious. CO_2 is injected in a zone of 125 m vertical and 50 m radial extent, representing not a single well, but rather a few distributed wells. Injection occurs over 30 years at a rate of 120 kg/s, corresponding to a large carbon source with an annual output of 3.8 million tonnes of CO_2. The aquifer is initially fully brine-saturated, assuming a hydrostatic fluid pressure distribution in the vertical direction. Isothermal conditions are modeled with a uniform temperature of 45ºC.

Values for hydrogeologic properties were assigned representative of a homogeneous brine formation suitable for CO_2 storage (Table 1). In the base case, the pore compressibility is 4.5×10^{-10} Pa^{-1}, a value representative of structurally sound sandstone (Harris, 2006), and the permeability of the isotropic storage formation is 10^{-13} m^2. Pore compressibility is a key property for a pressure-constrained aquifer, because it defines the pore space (or porosity) increase in response to pressure buildup, while permeability is a key property defining the movement and spatial distribution of CO_2. Note that the compressibility of brine is intrinsically taken into account in TOUGH2/ECO2N in terms of density variation with fluid pressure. Unlike many groundwater flow simulators, which employ specific storativity to describe the combined effect of pore and fluid compressibility, TOUGH2/ECO2N separates the effects of porosity change and density variation. Brine compressibility is mildly sensitive to pressure and temperature changes in the pressure-temperature range relevant to CO_2 storage. For the conditions at the aquifer top depicted in Figure 4, with a pressure of 120 bar and a temperature of 45ºC, brine compressibility is on the order of 3.5×10^{-10} Pa^{-1}.

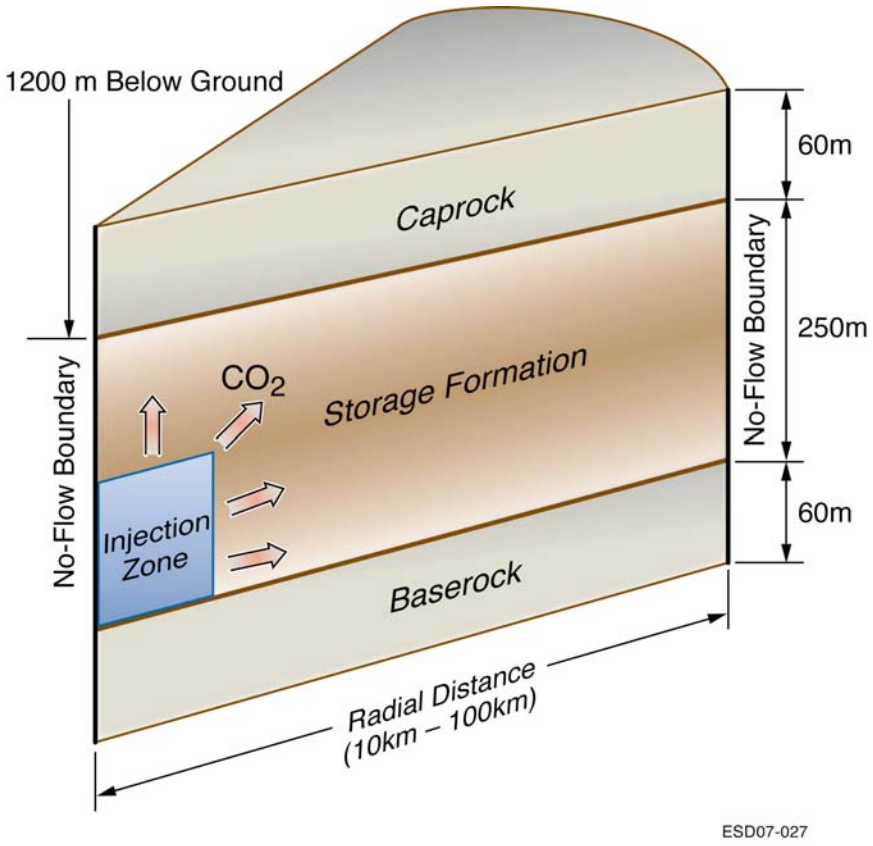

Figure 4. Schematic showing radially symmetric model domain with deep brine formation for CO_2 storage and overlying/underlying seals (not to scale)

Table 1. Hydrogeologic properties used for the storage formation in the base-case simulations

Properties	**Values**
Permeability (m^2)	10^{-13}
Pore Compressibility (Pa^{-1})	4.5×10^{-10}
Porosity	0.12
van Genuchten (1980) m	0.46
van Genuchten α (Pa^{-1})	5.1×10^{-5}
Residual CO_2 saturation	0.05
Residual water saturation	0.30

3.2.2. Sensitivity Analyses

The capacity of CO_2 storage in a pressure-constrained system depends on many factors, in particular the hydrogeologic properties of the storage formation and the confining units (e.g., permeability, porosity, and pore compressibility), and total pore volume of the storage formation (e.g., thickness and radial extent). A set of sensitivity simulations was conducted varying these hydrogeologic properties and the radial extent of storage formation (see Table 2). In each sensitivity case, only the property of interest was changed from the base-case value. Results are used in Section 3.5 to compare the capacity estimates and efficiency factors obtained through numerical simulations with those from the quick-assessment method. Some justification for the choice of sensitivity cases and the related property ranges is given below.

Table 2. Simulation runs for varying radial extents of storage formation, and different values for permeability of the storage formation, as well as permeability of the seals

	Case No	Radial Extent (km)	Formation Permeability (m^2)	Seal Permeability (m^2)
Base Case	Case 1	20	1.0×10^{-13}	0
Storage Formation Volume	Case 2	10	1.0×10^{-13}	0
	Case 3	30	1.0×10^{-13}	0
	Case 4	50	1.0×10^{-13}	0
	Case 5	100	1.0×10^{-13}	0
Formation Permeability	Case 6	20	1.0×10^{-12}	0
	Case 7	20	5.0×10^{-14}	0
Seal Permeability	Case 8	20	1.0×10^{-13}	1.0×10^{-20}
	Case 9	20	1.0×10^{-13}	1.0×10^{-19}
	Case 10	20	1.0×10^{-13}	1.0×10^{-18}
	Case 11	20	1.0×10^{-13}	1.0×10^{-17}

3.2.2.1. Formation Volume (Radial Extent)

We studied different storage formation sizes, with radial extent ranging from 10 km to 100 km, representing scenarios that, for the given injection volume, range from clearly pressure-constrained (because of limited capacity) to not pressure-constrained (because of large capacity). For example, we expect the 10 km case to experience a pressure buildup higher than a reasonable threshold, meaning that CO_2 injection would have to cease before the designated injection period. In such a system, the maximum storage efficiency would be smaller than the actual storage capacity needed to store the designated volume of CO_2. In contrast, we expect the 100 km case to experience almost no pressure buildup at the outer lateral boundary, meaning that the storage formation would respond to injection as would an open system with potential for brine to escape. In such a scenario, the maximum storage efficiency would be much larger than the actual storage capacity after 30 years of injection.

3.2.2.2. Formation Properties

Permeability of the storage formation is one of the key parameters for pressure-constrained systems, influencing both the uniformity of pressure buildup over the domain and the propagation velocity of the pressure pulse away from injection zone. For example, when the formation permeability is relatively small, the local pressure buildup near the injection zone may be a limiting factor in the storage-capacity estimates. On the other hand, larger permeabilities would tend to result in relatively uniform pressure buildup both near and away from the injection zone. A reasonable range of permeability values (from 5.0×10^{-14} to 1.0×10^{-12} m^2) was used in the sensitivity analysis.

Pore compressibility is another key parameter affecting the storage capacity of a pressure-constrained system. For brevity, this parameter has not been varied in the sensitivity analysis. Wide ranges of pore (or matrix) compressibility can be expected in field situations, depending on the subsurface material (e.g., Fjar et al., 1991; Domenico and Schwartz, 1998; Hart, 2000; Harris, 2006), having a significant effect on the potential

CO_2 storage capacity in pressure-constrained systems. For example, Domenico and Schwartz (1998) give ranges of compressibility values for different materials, such as less than 3.3×10^{-10} Pa^{-1} for sound rock, 3.3×10^{-10} Pa^{-1} through 6.9×10^{-10} Pa^{-1} for fractured rock, and 1×10^{-8} Pa^{-1} through 5.2×10^{-9} Pa^{-1} for dense sandy gravel. Even higher compressibilities can be expected in plastic or unconsolidated materials (e.g., on the order of 10^{-6} or 10^{-7} Pa^{-1} for plastic clay), which are, of course, not typically relevant for deep geological storage of CO_2. On the other end of the spectrum, the lowest compressibility value measured from laboratory tests by Hart (2000) is 7.0×10^{-11} Pa^{-1} for Berea sandstone.

3.2.2.3. Seal Properties

Preferred CO_2 geological storage sites have a caprock formation that acts as a sealing barrier to the buoyant fluid. In the case of supercritical CO_2 migrating upward into brine-saturated caprock, the sealing capacity is a function of both low permeability and high entry capillary pressure, which are generally well correlated. In other words, most seals of relatively low permeability also have a considerable capillary sealing capacity with respect to CO_2. With respect to the native brine, on the other hand, there is no capillary sealing capacity at the interface between storage formation and sealing units; the migration of brine is limited only by the permeability contrast. As a result, the leakage of native brine into over- and underlying seals can be significant, depending on pressure gradients and seal permeability, while CO_2 may be safely trapped because of the combined permeability and capillary barriers. Seal permeabilities can range over orders of magnitude. For example, shale permeabilities have been reported to range from 10^{-23} to 10^{-16} m^2 (Neuzil, 1994; Domenico and Schwartz, 1998; Hovorka et al., 2001; Hart et al., 2006). Hart et al. (2006) recently measured the permeability of shale aquitards of the Maquoketa Formation in Wisconsin, and found the permeability to range from 2.5×10^{-21} to 4.1×10^{-19} m^2, while Neuzil (1994) found a wider range, between 10^{-23} to 10^{-17} m^2.

To investigate the importance of brine migration through low-permeability cap- and base-rocks, we conducted simulations for the domain with a 20 km radial extent, allowing for vertical interlayer brine migration (semi-closed systems) using seal permeability values of 10^{-20}, 10^{-19}, 10^{-18}, and 10^{-17} m^2 (i.e., between 10^{-5} and 10^{-2} millidarcy). These values are to be compared to the 10^{-13} m^2 permeability for the storage formation. The porosity in the sealing units is 0.05, and the van Genuchten (1980) α value is 5.1×10^{-6} Pa^{-1} (representing roughly the inverse of entry pressure for the nonwetting phase). All other properties are identical to the storage formation. In the model, fixed pressure conditions equal to hydrostatic are set at the top of the upper seal and the bottom of the lower seal, representing a sink for brine that has migrated vertically through the seals. It is thus assumed that any overpressure developing within the storage formation diminishes within the cap- and base-rock units.

3.3. Quick-Assessment Method

We developed a simple method for assessing the storage capacity of pressure-constrained storage formations. CO_2 injection into these systems will lead to pressurization (pressure buildup), because an additional volume of fluid needs to be stored. The injected CO_2 displaces an equivalent volume of native brine, which may be (1) stored in the expanded pore space in the storage formation, (2) stored in the expanded pore space in the seals, and (3) leak through the seals into overlying/underlying formations. The quick-assessment method predicts the pressure-buildup history over a given injection period and the actual storage efficiency factor at the end of injection. Several simplifications and assumptions of both reservoir characteristics (geometric and hydrogeologic properties) and processes are outlined below. The validity of these assumptions is discussed based on the detailed simulation results presented in Section 3.4, and in Section 3.5, the quick-assessment estimates are compared to simulation results to check the accuracy and usefulness of the approach.

The method is designated to provide capacity estimates at early stages of site selection and characterization, when (1) quick assessments of multiple sites may be needed and when (2) site characterization data are rather sparse. More specifically, the estimated pressure increase caused by injection and storage of a specified volume of CO_2 can be compared to a sustainable pressure threshold, which is the maximum pressure that the formation can sustain without geomechanical damage. Alternatively, one may determine the maximum CO_2 volume that can be injected without jeopardizing the geomechanical structure of the formation-seal system. As pointed out below, we provide the quick-assessment method for systems with zero seal permeability (closed systems) as well as systems with small but non-zero permeability (semi-closed systems).

3.3.1. Simplifications and Assumptions

We assume an idealized formation-seal system with uniform thickness for both storage formation and seals (see Figure 4), using the following simplifications and assumptions:

- The formation for CO_2 storage is of a horizontal area A with radial extent R and thickness B_f. With a uniform initial porosity ϕ_f, the initial total pore volume is $V_f = \phi_f A B_f = \pi R^2 \phi_f B_f$. The formation has a closed lateral boundary at R.
- The storage formation has a uniform pore compressibility β_p, which includes the possible contribution of vertical formation expansion. Pore compressibility is constant over the relevant pressure range, from the initial hydrostatic pressure to the increased pressure value under final storage conditions.
- The upper and lower seals have the same horizontal area A as the storage formation. Both seals have identical thickness, B_s and uniform values for permeability k_s, porosity ϕ_s, and pore compressibility β_{ps}. The total pore volume of both seals is $V_s = 2\phi_s A B_s$.
- Brine compressibility, β_w, representing the change in brine density in response to pressure buildup, is assumed to be constant over the relevant range of pressure

conditions. Brine viscosity, u_w, dependent on temperature, pressure, and salinity, is also assumed to be constant during the CO_2 injection period.

- The pressure buildup in the storage formation is uniform, independent of formation permeability. The quick-assessment method calculates an expected average pressure in the storage formation, but does not consider local pressure increases near the injection zone.
- The entire formation-seal interface is in contact with brine (for the calculation of brine leakage), independent of CO_2 plume extent.
- The overpressure developed within the storage formation decreases linearly within the seals. The pressure at the top of the overlying seal and at the bottom of the underlying seal remains at hydrostatic conditions prior to CO_2 injection.
- All injected CO_2 mass is stored as a CO_2–rich phase, with negligible dissolved CO_2 mass, and CO_2 does not escape from the storage formation. This means that the total volume of stored CO_2 under the storage condition equals the total volume of displaced brine.

Note that the storage formation can have any shape with varying thickness, because only its total pore volume is used in the quick-assessment method. Specifications on the geometry of the storage formation have been employed for easier comparison with numerical simulation results.

3.3.2. Basic Equations

The quick-assessment method considers that the pore volume needed to store the injected CO_2 volume, $V_{CO2}(t_I)$, after a given injection time, t_I, is provided by three contributions: (1) the expanded storage volume in the storage formation resulting from pressure buildup, (2) the expanded storage volume within the seals resulting from pressure buildup, and (3) the volumetric leakage of brine into the formations above and below the upper and lower seals, respectively. The expanded storage volume is caused by

both brine and pore compressibility. A simple expression can be developed that describes this volumetric relationship, as follows:

$$V_{CO2}(t_I) = (\beta_p + \beta_w)\Delta p(t_I)V_f + 0.5(\beta_{ps} + \beta_w)\Delta p(t_I)V_s + \int_0^{t_I} \frac{2Ak_s\Delta p(t)}{\mu_w B_s} dt, \qquad (1)$$

where each of the three terms on the right-hand side corresponds to one of the three storage contributions mentioned above. Equation (1) essentially links the injected CO_2 volume to the average pressure buildup in the storage formation, with $\Delta p(t_I)$ being the pressure buildup at time t_I and $\Delta p(t)$ ($t = [0, t_I]$) being the transient pressure buildup from the beginning to the end of injection. By solving Equation (1) for t_I at the end of the injection period, the total pressure buildup in the closed or semi-closed formation can be assessed as a function of injected CO_2 volume. All three terms in Equation (1) need to be considered for semi-closed systems. For closed systems, Equation (1) reduces to the first term on the right-hand-side.

Based on the definition of efficiency factors and the relationship in Equation (1), the actual storage efficiency factor, $E(t_I)$, for a semi-closed system can be calculated as

$$E(t_I) = (\beta_p + \beta_w)\Delta p(t_I) + 0.5(\beta_{ps} + \beta_w)\frac{V_s}{V_f}\Delta p(t_I) + \int_0^{t_I} \frac{2k_s\Delta p(t)}{\mu_w \phi_f B_f B_s} dt, \qquad (2)$$

which, in analogy to Equation (1), has three individual efficiency contributions from increased pore space in the storage formation and the seals, as well as from brine leakage into the underlying and overlying formations.

To compare the relative importance of the three individual contributions to storage capacity, we may define the volumetric fractions of displaced brine stored in the storage formation (F_f), in the seals (F_s), and in the overlying/underlying formations (F_l), relative to the total injected CO_2, as follows:

$$F_f = (\beta_p + \beta_w)\Delta p(t_I)V_f / V_{CO2}(t_I), \qquad (3a)$$

$$F_s = 0.5(\beta_{ps} + \beta_w)\Delta p(t_1)V_s / V_{CO2}(t_1), \quad (3b)$$

$$F_l = \int_0^{t_1} \frac{2Ak_s \Delta P(t)}{\mu_w B_s} dt \Big/ V_{CO2}(dt). \quad (3c)$$

Per definition, F_f, F_s, and F_l add up to one.

The necessary CO_2 storage capacity for a given site is often provided in total mass, G_{CO2}, instead of total volume, V_{CO2}, as calculated from Equation (1). Conversion of volume to mass requires knowledge of the CO_2 density, ρ_{CO2}, evaluated at pressures and temperatures representing the final storage conditions. Because the pressure buildup caused by injection is not known beforehand for a given total CO_2 mass, the pressure-dependent CO_2 density at storage conditions is either estimated a priori (in anticipation of an estimated pressure buildup) or determined in an iterative procedure, using the calculated average pressure to correct the density and vice versa. (See Section 3.5.4 for a brief discussion of the potential inaccuracies related to the determination of CO_2 density.)

3.3.3. Application to Closed Systems

In a closed system with impervious seals, brine cannot escape from the storage formation into and through the seals. The available volume for storage of CO_2 is then provided only by the expansion of the pore volume, plus the increased brine density, in response to pressure buildup in the formation. Equation (1) can then be simplified to the following linear expression:

$$V_{CO2}(t_1) = (\beta_p + \beta_w)\Delta p(t_1)V_f \quad . \quad (4)$$

This equation can be used, for example, to estimate the maximum storage capacity for a given maximum sustainable pressure buildup, $\Delta p_{\max}$. Similarly, one can calculate the expected average pressure buildup, $\Delta p(t_1)$, for a given total volume of stored CO_2.

The efficiency factor of CO_2 storage in a closed system with average pressure buildup $\Delta p(t_I)$ can be derived from a simplification of Equation (2)

$$E = E_p(\Delta p(t_I)) + E_b(\Delta p(t_I)) = (\beta_p + \beta_w)\Delta p(t_I), \quad (5)$$

where E_p is the storage efficiency factor caused by pore compressibility, and E_b is the storage efficiency factor produced from brine compressibility. Inserting the maximum sustainable pressure buildup, $\Delta p_{\max}$, into Equation (5) results in the maximum storage efficiency of a closed system. For example, using a sustainable pressure buildup of $\Delta p_{\max} = 60$ bar, a pore compressibility of 4.5×10^{-10} Pa^{-1} (the value used in the numerical simulations) and a brine compressibility of 3.5×10^{-10} Pa^{-1}, we arrive at individual efficiency factors of E_p = 0.0027 and E_b = 0.0021, and a total storage efficiency of E = 0.0048. In other words, less than half a percent of the total pore volume of a closed system would be available for storage of CO_2 in a closed system.

3.3.4. Application to Semi-Closed Systems

For closed systems with impervious seals, the total volumetric storage capacity and pressure buildup at the end of injection are related in a simple linear manner to pore and brine compressibilities, as well as initial pore volume. For a semi-closed system with permeable seals, the capacity-pressure relationship in Equation (2) is nonlinear and transient, with the pressure buildup in the storage formation affecting leakage rate through the seals and vice versa. The stronger the pressure buildup, the higher the leakage rate, which in turn slows down the pressure buildup. This makes solving of Equation (1) more complicated; however, a solution can be achieved through a simple numerical integration in time. For this purpose, the injection time period $[0, t_I]$ can be discretized into a number (n) of equally spaced time intervals of duration Δt to form a time series: $t_0, t_1, ..., t_{i-1}, t_i, ..., t_{n-1}, t_n$, with $t_0 = 0$ and $t_n = t_I$. Equation (1) converts into its discrete form as follows

$$\Delta p(t_i) = \frac{V_{CO2}(t_i) - \dfrac{2Ak_s\Delta t}{\mu_w B_s}\sum_{j=0}^{i-1}\Delta p(t_j)}{(\beta_p + \beta_w)V_f + 0.5(\beta_{ps} + \beta_w)V_s + \dfrac{Ak_s\Delta t}{\mu_w B_s}}\ ,\ i = [1,\ n]\,. \qquad (6)$$

At each new time step, the pressure-buildup values at all previous time steps are known, such that the summation term in Equation (6) (representing the cumulative brine leakage from beginning of injection to the previous time step) can be executed. This eventually yields the pressure buildup at all time steps from the beginning to the end of injection. Once Equation (6) has been solved, the efficiency factors in Equation (2) or the volume fractions in Equation (3) can be derived using the known injection and pressure history.

Note that continued CO_2 injection into a semi-closed system would eventually lead to a steady-state condition at which the volumetric injection rate, Q_{CO2}, equals the rate of brine leakage through the seals. The pressure buildup, Δp_S, associated with this steady-state condition can be calculated as follows:

$$\Delta p_S = \frac{Q_{CO2}}{2Ak_s / \mu_w B_s}\,. \qquad (7)$$

If Δp_S is unrealistically high, i.e., higher than the sustainable pressure buildup, the storage capacity is pressure constrained and needs to be evaluated, using Equation (6). If, on the other hand, Δp_S is relatively small, brine leakage through the seals is efficient enough to allow for sufficient CO_2 storage without pressurization concerns. In this case, the semi-closed system acts like an open storage formation, and its storage capacity is not pressure-constrained.

3.3.5. Sustainable Pressure Buildup

The CO_2 storage capacity of pressure-constrained systems depends on the maximum pressure buildup that a given formation is expected to tolerate. In most applications, this sustainable pressure buildup will be based on geomechanical considerations, with the goal of avoiding degradation (such as microfracturing and/or fault reactivation) of the

sealing structures (EPA, 1994; Rutqvist and Tsang, 2002; Rutqvist et al., 2007a, 2007b; Neuzil, 2003). Fluid pressure in the storage formation may also be constrained to limit the pressure driving forces into neighboring formations, or to account for potential concerns about seismicity. According to Rutqvist et al. (2007a), the sustainable pressure buildup should be reviewed in a case-by-case assessment, taking into account initial stress fields and geomechanical properties of the rock units at the selected sites.

Some guidance on the determination of a ustainable pressure-buildup threshold is provided by the current practice for underground injection control of liquid wastes. The regulatory standard states that maximum injection pressure should be less than the measured fracture closure pressure, below which any existing fractures cannot open, no new fractures can form, and therefore neither can transmit waste fluids out of the injection intervals (EPA, 1994). The regional guidance for implementation is that the maximum injection pressures can be determined either by a site-specific fracture closure pressure derived from direct or indirect testing, or by formation-specific default values for the fracture-closure pressure gradients. For example, a default value of 0.57 psi/ft (132% of the hydrostatic pressure gradient) is given for the Mt. Simon Formation; 0.8 psi/ft (185% of the hydrostatic pressure gradient) is reported for the Dundee Limestone. For the hypothetical example studied in this report, with a formation depth of 1,200 m to 1,450 below the ground surface, these default fracture-closure pressure gradients correspond to sustainable fluid pressures of 158 and 222 bar, respectively (at 1,200 m depth). This translates to pressure buildup values between 38 and 102 bar. In our application example, we assume a sustainable pressure buildup threshold of 60 bar, which corresponds to 50% of the initial hydrostatic pressure at the top of the hypothetical storage formation.

3.4. Simulation Results and Discussion

Results from the numerical simulation examples introduced in Section 3.2 are presented here, with focus on the migration of the CO_2 plume and the evolution of pressure buildup. Sensitivity to various hydrogeological and geometrical properties is investigated, and their impact on CO_2 storage capacity is discussed.

3.4.1. Spatial and Temporal Distributions of CO_2 Plume and Pressure Buildup

Figure 5 shows the spatial distributions of CO_2 saturation, CO_2 density, fluid pressure, and pressure buildup (compared to the initial hydrostatic pressure distribution) at the end of the 30-year injection period. The presented results are for the base case with a model domain extending 20 km and impermeable upper and lower seals. The CO_2 plume is approximately 4 km wide and is concentrated at the top portion of the aquifer, a result of the buoyant CO_2 accumulating below the impervious caprock (Figure 5a). The density of the supercritical CO_2 varies slightly, from 820 kg/m^3 at the bottom of the reservoir to 780 kg/m^3 at the top, caused by local pressure differences (Figure 5b).

As shown in Figures 5c and 5d, the region of elevated pressure is much larger than the CO_2 plume size. In fact, a substantial pressure increase from hydrostatic is observed throughout the entire 20 km model domain, with the pressure buildup at the outer radial boundary at approximately 45 bar. Since the displaced brine cannot escape from the storage formation, the entire domain becomes an overpressured system, with the storage capacity provided by pore and fluid compressibility in response to the pressure increase. In addition to the formation-scale pressure buildup, there is some local increase near the injection zone, creating a driving force for the displacement of brine. The total pressure buildup near this zone is slightly above 60 bar, thus exceeding the sustainable pressure threshold assumed for this formation. We may conclude that this example features a pressure-constrained formation near or slightly beyond its capacity limits at the end of the designated injection time. Notice that the pressure contour lines away from the injection zone are mostly vertical, indicating horizontal brine displacement. Nonvertical contour

lines can be seen in the CO_2 plume region, where the pressure conditions are affected by buoyancy, as well as nonlinearity due to two-phase flow processes.

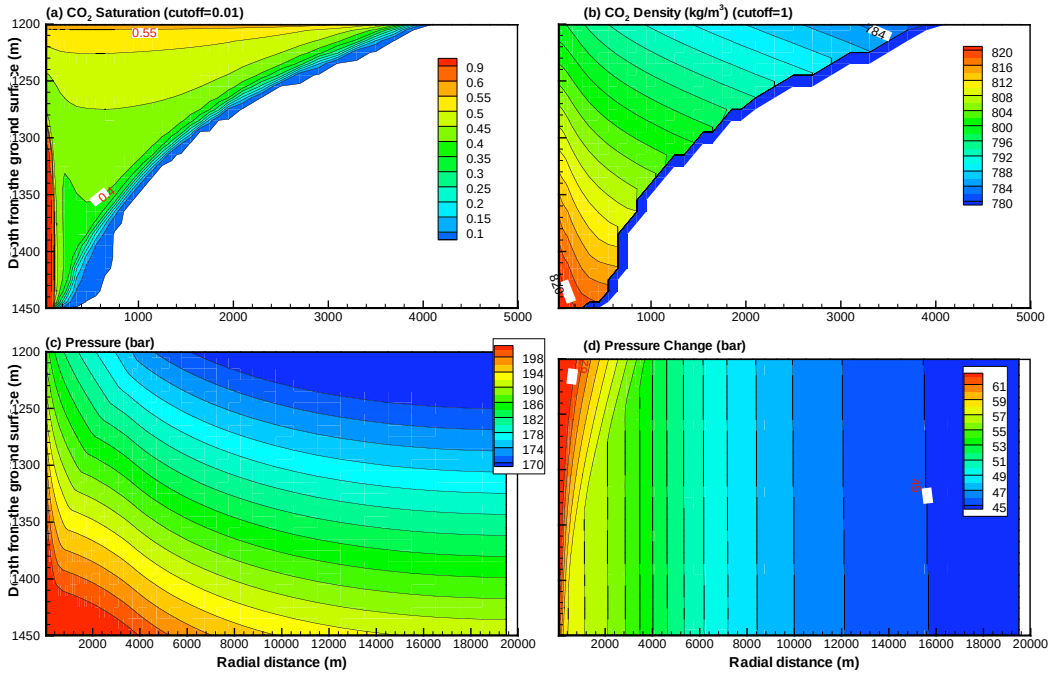

Figure 5. Spatial distribution of (a) CO_2 saturation, (b) CO_2 density, (c) fluid pressure, and (d) pressure buildup (change in fluid pressure from the initial hydrostatic condition), at 30 years of CO_2 injection, simulated for the "closed" domain with a 20 km radial extent. Figures 5a and 5b show close-ups of the CO_2 plume (region with two-phase flow of CO_2 and brine).

Radial pressure-buildup profiles at different times throughout the injection period are shown in Figure 6. At the very beginning of injection, the injected CO_2 displaces native brine in the area very close to the injection zone. The strong initial pressure buildup is the driving force to (1) move native brine away from the injection zone and (2) to overcome phase interference between aqueous and CO_2 phases in the region of two-phase flow (Pruess and Garcia, 2002). This pressure increase, referred to here as *injection-driven pressure buildup*, depends on the boundary condition (i.e., CO_2 injection rate in the injection zone, injection strategy), formation permeability, and two-phase flow conditions; its extent coincides roughly with the radial extent of the CO_2 plume. The pressure pulse propagates away from the injection zone and reaches the outer radial boundary after approximately 2 years. After that, since the displaced brine cannot escape, the pressure at the outer boundary starts to increase with injection time in an

approximately linear manner; i.e., the entire model domain becomes overpressured such that additional pore volume is made available to store the injected CO_2. The pressure buildup related to the need for generating additional pore space is referred to as *storage-driven pressure buildup*, which depends mainly on the pore compressibility of the formation (as well as on changes in brine density).

Both injection-driven and storage-driven pressure changes define the eventual pressure buildup that the formation experiences, with the relative importance of injection-driven buildup decreasing as time progresses. As discussed above, the final pressure conditions in this example simulation exhibit pressure increases over the majority of the model domain that are less than the sustainable threshold of 60 bar. Only in the region less than one kilometer away from the injection zone is the pressure buildup slightly higher than the threshold. Adequate injection strategies may be employed in such cases to reduce the injection-driven contribution to the pressure increase.

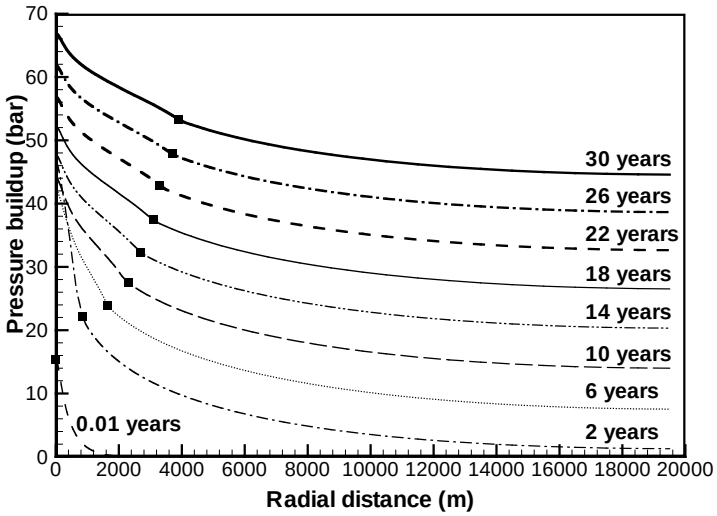

Figure 6. Pressure-buildup profiles along the aquifer top at different injection times. Symbols indicate the CO_2 plume extent to show the radial extent of the evolving two-phase flow region.

3.4.2. Variation of Formation Volume (Radial Extent)

Figure 7 shows the spatial distribution of saturation and pressure buildup at the end of the 30-year injection period for the case of a model domain with 100 km radial extent.

Comparison of Figures 5a and 7a indicates that the CO_2 plumes in both cases, with 20 km and 100 km radial extent, are generally similar in shape. Minor differences can be seen in the lateral extent of the plumes, because differences in the pressure increases give rise to differences in CO_2 density. Remember that the total CO_2 mass injected into the formation is the same at the end of the 30-year injection for both cases. In contrast to the small difference in CO_2 plume extent, a significant difference in the pressure conditions is observed between the two cases. The larger model domain is not pressure-constrained, as indicated by the zero pressure increase at the outer radial boundary at 100 km. In other words, the pressure conditions represent those of an open system, where the lateral boundary is too far away to be affected by any pressure perturbation or brine displacement. As a result, the maximum pressure increase near the injection zone, about half of what is observed in the 20 km case, represents injection-driven pressure buildup without any contributions from storage-driven pressure increases. At a radial distance of 20 km, the pressure buildup is 8 bar in the 100 km case, significantly lower than the 45 bar observed in the 20 km case.

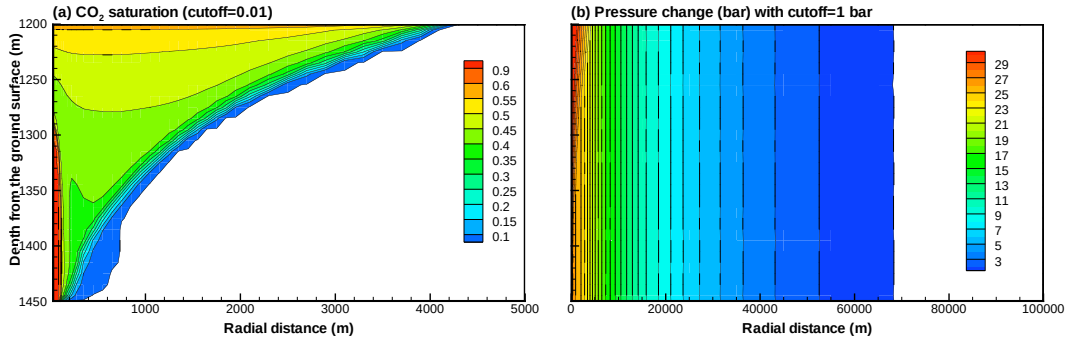

Figure 7. Spatial distributions of (a) CO_2 saturation and (b) pressure buildup at 30 years of CO_2 injection, simulated for the "closed" system with a 100 km radial extent. Figure 7a shows a closeup of the CO_2 plume (region with two-phase flow of CO_2 and brine).

Figure 8 shows pressure-buildup profiles along the aquifer top for all five sensitivity cases with different formation volumes. We observe that the pressure evolution is identical for all cases as long as the pressure pulse has not reached the respective model domain boundary. Once the pressure pulse reaches the lateral boundary, the pressure

increases at the boundary and the profiles start to deviate from the other cases with larger radial extent (which still act similar to open systems). In Figure 8, this behavior can be seen after 2 years of injection in the 10 km case, after 4 years in the 20 km case, after 8 years in the 30 km case, and after 30 years in the 50 km case. Clearly, the smaller the formation, the sooner the pressure profiles start to deviate from the other results, and the higher the overall pressure buildup at the end of injection period. In the 10 km case, the simulated total pressure buildup actually reaches an unrealistically high level at the end of 30-year injection, with maximum values above 180 bar (beyond the scale of the vertical axis in Figure 8d). Injection would have to cease after approximately 8 years to keep the actual pressure buildup smaller than the sustainable threshold of 60 bar.

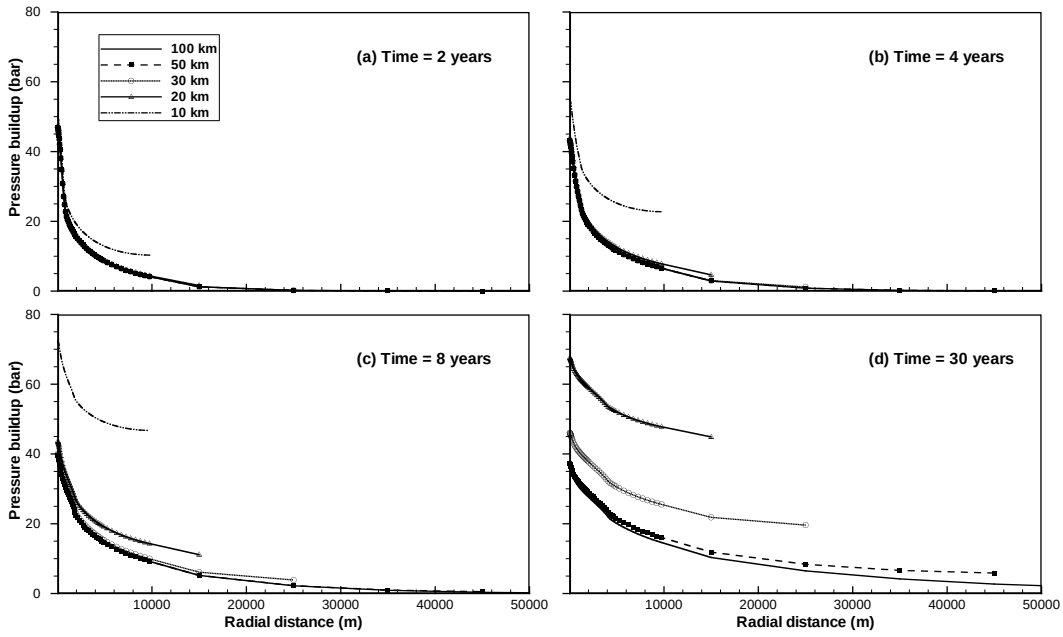

Figure 8. Pressure-buildup profiles along the aquifer top for different radial extents at (a) 2, (b) 4, (c) 8, and (d) 30 years of CO_2 injection

3.4.3. Variation of Formation Permeability

Figure 9 shows the sensitivity of local pressure buildup to the permeability of the storage formation. For the case with higher permeability (one order of magnitude higher than base case), the pressure buildup in the formation is almost uniform over the entire area,

varying from 51 bar close to the injection zone to 47 bar at the outer boundary (Figure 9a). This uniformity would increase the storage capacity of a pressure-constrained formation, because the contribution of local pressure buildup due to injection is comparably small. For the second case with a lower permeability (a factor of two smaller than the base case), a strong local pressure buildup near the injection zone leads to total fluid pressure in excess of the assumed sustainable threshold of 60 bar—see Figure 9b. This condition occurs over most of the injection period, even at early times when the pressure pulse has not reached the model boundary.

As mentioned in Section 3.3, the quick-assessment method assumes a uniform pressure buildup in the pressure-constrained storage formation, thereby accounting for storage-driven pressure buildup, but not for injection-driven pressure buildup. It follows that the method would not provide meaningful results when the maximum pressure threshold is exceeded, because of injection constraints rather than volumetric storage constraints. Clearly, the pressure profiles observed in Figure 9b are good examples for such conditions. Thus, in closed systems with rather small permeability, the local pressure buildup would need to be considered by alternative methods, e.g., using detailed numerical models.

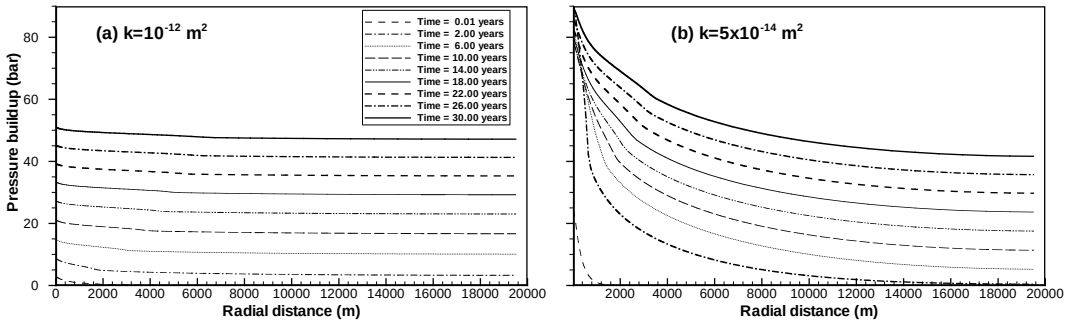

Figure 9. Horizontal profiles of pressure buildup at different times of CO_2 injection for formation permeability of (a) 10^{-12} and (b) 5×10^{-14} m^2

3.4.4. Variation of Seal Permeability

Figure 10 shows horizontal profiles of pressure buildup in the model domain considering different permeability values assigned to the sealing units. In contrast to the impermeable seals assumed in the base case (closed systems), we now use permeability values of 10^{-20}, 10^{-19}, 10^{-18}, and 10^{-17} m^2, respectively (semi-closed systems). The pressure buildup

observed in the storage formation is very sensitive to increases in seal permeability. While the lowest seal permeability shows a behavior very similar to the closed system, we see a strong reduction of overall pressure buildup in all other cases, particularly those with permeabilities of 10^{-18} and 10^{-17} m^2. In these cases, a significant fraction of the displaced brine escapes from the storage formation into the seals, and through the seals into the overlying and underlying formations, thereby providing additional storage capacity for the injected CO_2 such that less pressure buildup occurs.

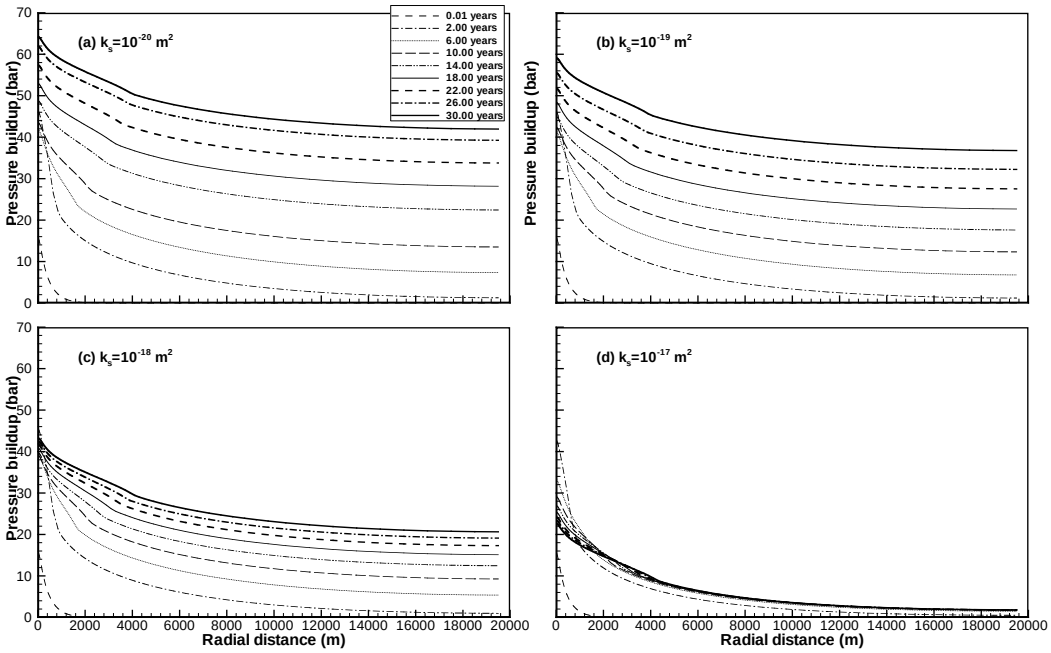

Figure 10. Horizontal profiles of pressure buildup along the aquifer top at different times of CO_2 injection for seal permeability of (a) 10^{-20}, (b) 10^{-19}, (c) 10^{-18}, and (d) 10^{-17} m^2

We have calculated the cumulative fraction of displaced brine escaping from the storage formation relative to the total volume of injected CO_2. With a small seal permeability of 10^{-20} m^2, this volume fraction is rather insignificant at 0.07, whereas with a seal permeability of 10^{-17} m^2, this fraction increases to 0.93; i.e., the additional CO_2 storage capacity from brine leakage would amount to about 93% of the totally injected CO_2 after 30 years. This effect can be very important for storage-capacity estimates in compartmentalized systems that have sealing units with small, but non-zero,

permeability. Notice that the pressure profiles in Figure 10d (for a seal permeability of 10^{-17} m^2) remain relatively unchanged after a few years of injection, indicating that a quasi-steady state has been reached in which the volumetric rate of leakage of displaced brine is identical to the volumetric rate of injected CO_2.

In contrast to the significant leakage of displaced brine, insignificant amounts of CO_2 escape from the storage formation into the seals. The cumulative fractions of CO_2 leaking into the caprock are 0.22%, 0.35%, 0.70%, and 3.1% of the total injected CO_2 mass, for the seal permeability cases of 10^{-20}, 10^{-19}, 10^{-18}, and 10^{-17} m^2, respectively. This is because CO_2 as the nonwetting-phase fluid needs to overcome a considerable capillary entry pressure before being able to migrate into the water-saturated pores of the sealing units. Notice also that the observed migration of CO_2 within the seals is limited to the immediate vicinity of the storage formation; CO_2 is not able to escape into units overlying or underlying the seals. Our results thus suggest that compartmentalized storage reservoirs with reasonably good, but not perfect, seals may allow for enough brine leaking out of the formation to offset pressure-related storage limitations, while still having sufficient sealing capacity to trap supercritical CO_2.

3.5. Validity of the Quick-Assessment Method

This section describes application of the quick-assessment method to the simulation scenarios discussed above. We derive estimates for domain-averaged pressure buildup and storage efficiency factors and compare these with the corresponding “true” values obtained via detailed numerical simulations.

3.5.1. Comparison of Pressure-Buildup Estimates

The first step to demonstrate the validity of the quick-assessment method is to compare the estimated domain-averaged pressure buildup against the numerical simulations results for both closed and semi-closed systems. Figure 10a shows domain-averaged pressure buildup, as a function of injection time, for closed systems (with impermeable seals) of

varying total pore volume. The quick-assessment estimates have been obtained using Equation (4), solving for pressure buildup $\Delta P(t)$ at given times t during the injection period. The corresponding cumulative CO_2 volume $V_{CO2}(t)$ at each time step t is derived from the constant CO_2 injection rate of 120 kg/s used in the examples. Conversion from CO_2 mass to CO_2 volume is conducted at each time step using the CO_2 density at average pressure conditions, which, as mentioned before, requires a few iterations. The estimated results are then compared to the domain-averaged pressure values derived from the numerical simulations. The agreement between the true numerical solutions and the quick estimates is excellent, considering that several simplifications and assumptions are involved in the quick-assessment method (e.g., uniform pressure buildup in domain, no dissolution, constant compressibility values).

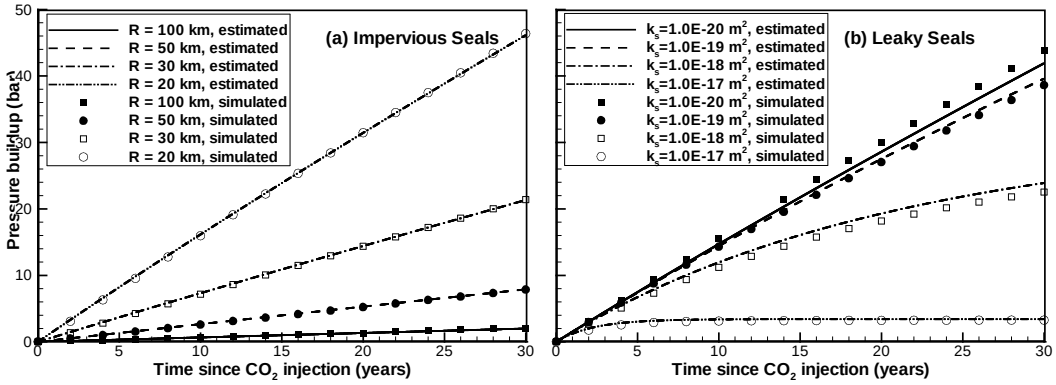

Figure 11. Comparison of the transient profiles of domain-averaged pressure buildup obtained through numerical simulations and through the quick-assessment method for (a) a closed system with varying radial extents R, and (b) a semi-closed system with radial extent R = 20 km and seals of varying seal permeability (k_s).

Figure 11b shows a similar comparison of domain-averaged pressure buildup for the semi-closed system with non-ideal seals of varying permeability. In this case, the quick-assessment estimates are obtained using Equation (6). Overall, the agreement between estimated and numerical results is reasonably good, with a maximum discrepancy of less than 6%. While the quick-assessment method captures the general nonlinear trends in pressure buildup very well, it slightly underestimates pressure buildup for the case with

the smallest seal permeability (i.e., 1.0×10^{-20} m^2) and slightly overestimates pressure buildup in the cases with relatively high seal permeability (i.e., 1.0×10^{-17} m^2).

In summary, the quick-assessment method provides reliable pressure estimates, ones that can be compared with the maximum sustainable pressure buildup to judge whether the designated volume of CO_2 can be safely stored in a storage formation with or without vertical interlayer communication with other units.

Both numerical and estimated results show clearly that the average pressure approaches an asymptotic maximum after a few years in the case with the relatively high seal permeability of 10^{-17} m^2 (Figure 11). As mentioned before, this indicates a steady-state condition with equal rates of CO_2 entering and brine leaving the storage formation. We apply Equation (7) to calculate the average pressure buildup that would correspond to such a condition and arrive at values of 3.4, 32.3, and 270.2 bar for the three cases with seal permeabilities of 10^{-17}, 10^{-18}, and 10^{-19} m^2, respectively. In the first case, as to be expected, the estimated value from Equation (7) is identical to the final pressure buildup shown in Figure 11b. In the second case, a steady-state condition has not yet been established after 30 years of injection, but would be reached if injection would continue for a few more years. The pressure value of 32.3 bar associated with this steady-state condition is less than the sustainable pressure threshold, indicating that this scenario would not be pressure-constrained even if the injection period were much longer. In the third case, however, with a seal permeability of 10^{-19} (or less), a steady-state condition cannot be reached without geomechanical degradation of the seals, because the steady-state pressure buildup calculated from Equation (7) is much higher than the sustainable threshold.

3.5.2. Comparison of Efficiency Factors for Closed Systems

We now compare the simulated and estimated efficiency factors of CO_2 storage in a closed system with varying total pore volume (i.e., radial extents of 10, 20, 30, 50, 100 km). As pointed out before, the efficiency factor is defined as the cumulative volume of CO_2 per total initial pore volume. We calculate "actual" efficiencies, meaning we derive efficiency factors for the considered injection scenarios using the observed pressure buildup, independent of how this relates to a maximum sustainable pressure buildup. Notice that the simulated efficiency factors include storage contributions from CO_2 in supercritical phase as well as CO_2 dissolved in brine. The quick-assessment estimates are determined based on the average pressure buildup from the simulation runs, then using Equation (4) to calculate the total injected CO_2 volume or Equation (5) to directly calculate the actual efficiency.

Table 3 shows the comparison of the actual efficiency factors for each case after 30 years of injection, showing reasonable agreement between estimated and calculated results. The quick-assessment estimates are slightly higher than those obtained through detailed numerical simulations. It can be seen that the average pressure buildup in the 20 km case is close to the sustainable pressure-buildup threshold (60 bar), whereas the pressure buildup in the larger domains is far less than the threshold, resulting in significantly smaller actual storage efficiencies. In comparison, the maximum storage efficiency, calculated using the sustainable pressure buildup of 60 bar and assigning reasonable values for brine and pore compressibilities would be E = 0.0048 (Section 3.3.3). The calculated actual efficiency factors can be evaluated against the maximum efficiency factor to check whether the designated CO_2 volume can be safely stored. For the case of 10 km radial extent, the pressure buildup at the end of the 30-year injection period is clearly higher than the sustainable threshold, indicating that the designated CO_2 volume is not feasible in this case.

Table 3. Comparison of the actual efficiency factors for CO_2 storage in a closed system, using numerical simulation results and the quick-assessment method in Equation (5), at 30 years of injection

		Simulation-Based Results			Quick-Assessment Estimates
Domain Radius (km)	Initial Pore Volume (10^9 m^3)	Total Stored CO_2 Volume[1] (10^9 m^3)	Average Pressure Buildup Δp (bar)	Actual Efficiency Factor	Actual Efficiency Factor
100	942.5	0.139	2.0	0.00015	0.00017
50	235.6	0.138	7.9	0.00059	0.00066
30	84.8	0.136	21.4	0.0016	0.0018
20	37.7	0.131	46.4	0.0035	0.0039
10	9.4	0.117	166.0[2]	0.0124	0.014[2]

[1] Injected mass is identical for all domains. Stored volumes differ slightly because of different pressure/density conditions.

[2] Average pressure buildup is higher than sustainable threshold. The calculated actual storage efficiency is therefore not feasible.

3.5.3. Comparison of Storage Contributions for Semi-Closed Systems

In this validation exercise, we analyze the three individual contributions to CO_2 storage capacity in semi-closed systems, provided by native brine within the storage formation, in the seals, and in the overlying/underlying formations. Values obtained through the quick-assessment method (using Equations 3a through 3c) are compared against those directly derived from the numerical simulations. Table 4 summarizes the resulting volumetric fractions for the different seal permeability cases at the end of the 30-year injection period. One can see that most of the storage capacity is provided by the storage formation when seal permeability is small (e.g., more than 90% for seal permeability of 10^{-20} m^2). In contrast, most of the storage capacity is provided by brine escaping through the seals when seal permeability is comparably high (e.g., more than 90% for seal permeability of 10^{-17} m^2). In all cases, the match between the simulated and estimated fractions is reasonably good. The largest relative discrepancies occur with respect to the seal storage of displaced brine, which fortunately is the least important of the three contributions. As discussed in Section 3.3.1, seal storage is calculated assuming a linear pressure variation

in the seals at all times, a condition that may be violated in certain cases. In the small-permeability case (i.e., 10^{-20} m^2), for example, the pressure pulse penetrates only halfway through the seals within the injection period, clearly exhibiting a nonlinear behavior.

Table 4. Comparison between simulated and estimated volumetric fractions of displaced brine stored in the storage formation, in the seals, and in the overlying and underlying formations, relative to the total injected CO_2 at the end of the 30-year injection period, for different seal permeability values

Seals Permeability	Simulation Results			Estimation by Equation (3)		
	Storage Formation	Seals	Other Formations	Storage Formation	Seals	Other Formations
10^{-17} m^2	0.071	0.011	0.918	0.069	0.007	0.925
10^{-18} m^2	0.470	0.104	0.426	0.500	0.050	0.450
10^{-19} m^2	0.824	0.150	0.026	0.850	0.085	0.065
10^{-20} m^2	0.931	0.059	0.010	0.903	0.090	0.007

3.5.4. Adequacy of Important Assumptions and Simplifications

As the above comparisons show, the quick-assessment method provides reasonable estimates for the CO_2 storage capacity and pressure buildup in compartmentalized saline formations with impervious or non-ideal seals. One major limitation is the assumption of a uniform pressure buildup throughout the entire storage formation. This assumption works well as long as the average pressure is reasonably representative of the true pressure conditions (or, in other words, if the injection-driven pressure buildup is less important than the storage-driven pressure buildup). The detailed simulations in Section 3.4.3 feature one sensitivity case with small formation permeability of 5×10^{-14} m^2, where injection pressure alone exceeds a sustainable threshold. The quick-assessment method is not applicable in this case. We generally recommended judging the quick-assessment results with care, knowing that the average pressure predictions may underestimate the local conditions near the injection zone.

Inaccuracies related to the fluid properties employed in the quick-assessment method can be quantified. For example, brine viscosity and compressibility are assumed constant. The inaccuracies introduced by this assumption are negligible over the pressure range relevant in this study. CO_2 density is either assumed constant or is calculated based upon the actual domain-averaged pressure values at storage conditions. The latter captures transient pressure changes better than the former, but still introduces some inaccuracies because the domain-averaged pressure buildup may differ from actual pressure conditions within the CO_2 plume (which, of course, define CO_2 density). For the pressure range evaluated in this study (i.e., from 120 bar at hydrostatic to 180 bar at sustainable maximum pressure), the CO_2 density varies between 720 and 820 kg/m^3 (at 45ºC), a difference of about 12%.

A similar uncertainty contribution is introduced by the assumption of negligible CO_2 dissolution. This assumption leads to an overestimation of pressure buildup and an underestimation of CO_2 storage capacity. The approximation error caused by this assumption depends on the CO_2 solubility in brine, which in turn varies with pressure, temperature, and salinity. The error also depends on the fraction of CO_2 in contact with water. The detailed numerical simulations presented in this study suggest that the mass fraction of CO_2 dissolved in brine (with salt mass fraction of 0.15) ranges from 0.02 to 0.03, and that the dissolved CO_2 accounts for approximately 7% of the total injected CO_2 mass at the end of the 30-year injection period.

3.5.5. Storage Capacity in Closed and Open Systems

The maximum efficiency factor of CO_2 storage in a closed formation is relatively small. In the examples discussed in this study, the maximum storage efficiency is on the order of 0.005 (or 0.5% of the total initial pore volume), using a pore compressibility value typical of sedimentary rock and assuming a maximum pressure buildup of 60 bar. As discussed in Section 3.2.2.2, pore compressibility can vary widely depending on the formation materials. Pore compressibility values ranging from 4.5×10^{-11} Pa^{-1} to $4.5 \times$

10^{-9} Pa^{-1} would translate to maximum efficiency factors ranging from 0.0025 to 0.029 (0.25% to 2.9%). The efficiency in a closed system is smaller than these maximum values when local pressure increase is relevant and injection-driven pressure contributions would need to be added to the domain-averaged pressure estimates. On the other hand, CO_2 dissolution in brine allows for more carbon storage in a closed system than predicted by the quick-assessment method. Inclusion of dissolution would increase storage efficiency on the order of a few to ten percent.

In semi-closed systems, brine leakage into and through the seals can significantly enhance the storage capacity of a formation. Our simulations indicate that in cases with a comparably high seal permeability (in our application example around 10^{-19} m^2), the rate of brine leakage through the seals is sufficient to significantly reduce pressure buildup in the storage formation (while the capillary and permeability barriers capabilities of the seals are still effective in containing injected CO_2 in the storage formation). For larger seal permeabilities, on the order of 10^{-17} m^2, the formation-seal system effectively acts like an open system, where storage-driven pressure buildup is no longer a constraint on storage capacity estimates.

Capacity estimates for open systems have focused on determining the limits on CO_2 pore occupancy owing to hydrodynamic, heterogeneity, gravity, and multiphase effects. DOE (2007) considered so-called formation-scale contributions, reducing the net pore volume available for CO_2 storage in a suitable formation, defining individual efficiency factors for areal displacement effects (0.5–0.8), vertical displacement effects (0.6–0.9), gravity effects (0.2–0.6), and microscopic displacement effects (0.5–0.8). Multiplication of these individual factors provides first-order estimates on the overall storage efficiency range in an open formation. For example, multiplying the respective minimum and maximum factors given above, one arrives at an efficiency range for open systems from 0.03 up to 0.35. This range is much higher than the range (0.0025 to 0.029) for a closed system, as considered above. Of course, issues related to pressure buildup or brine displacement are

not considered in the open-system estimates developed in DOE (2007), i.e., there is an intrinsic assumption that the storage capacity is not constrained by pressure buildup or brine displacement and the possible impact on the environment.

3.6. Summary for Pressure-Constrained Systems

1) The available volume for CO_2 storage in closed/semi-closed systems is mostly provided by pore compressibility and brine compressibility in response to formation pressure buildup, and areal leakage of native brine into and through seals.

2) Methods for quick assessment of pressure buildup and storage capacity were developed for storage formations with impervious as well as permeable seals. The validity of these methods was demonstrated through reasonable agreement with results from detailed numerical simulations. The quick-assessment methods estimate the expected pressure buildup in response to injection of a given volume of CO_2, which can then be compared to a sustainable pressure buildup threshold in the formation. The threshold pressure values are usually selected based on geomechanical assessments or regulatory considerations. Simplifications and assumptions are made that may limit the applicability of the method is certain cases. See Section 3.5.4 for a discussion.

3) For a closed system with impervious seals, a typical formation-scale maximum efficiency factor of 0.005 was estimated for the conditions studied in this report, with similar storage contributions provided by pore and brine compressibility. Compared to this, DOE (2007) suggests formation-scale efficiency factors in open systems between 0.03 and 0.35, with a best estimate of 0.13.

4) One interesting finding of this research is the importance of seal permeability on pressure buildup in the storage formation. Closed systems with impermeable seals allow CO_2 storage only to the point that pressure in the formation approaches a given pressure threshold. This pressure constraint translates into small storage efficiency.

However, only formation-seal systems with very small seal permeability of 10^{-20} m^2 or less exhibit such a closed-system behavior; i.e., only then is the displacement of native brine into and through the bounding seals so small that the observed pressure buildup is similar to a closed system. In other sensitivity cases, with seal permeability varying from 10^{-19} m^2 to 10^{-17} m^2, brine leakage into and through the seals had a moderate to strong effect in reducing or limiting the pressure buildup in the storage formation, thus allowing for considerably higher storage efficiency (while CO_2 was still safely trapped because of the combined capillary and permeability barriers). Our results indicate that a semi-closed system with seal permeability of 10^{-17} m^2 is essentially an open system with respect to pressure buildup, because the rate of brine leaking through the seals equals the rate of injected CO_2 after a certain injection time period.

5) Related research results are being published in Zhou et al. (2007a,b) and Zhou et al. (in review), see Section 8.

4. Idealized Open Storage Formations

This section describes numerical modeling to estimate the region of influence in response to industrial-scale CO_2 injection in a large laterally open storage formation. Detailed numerical simulations have been conducted using the TOUGH2/ECO2N simulator (Pruess et al., 1999; Pruess, 2005) assuming a multilayer groundwater system with a sequence of aquifers and aquitards. We evaluated the region of influence in both lateral and vertical directions, by analyzing the pressure response as well as estimating the potential brine migration pathways. Sensitivity studies have been conducted varying the hydrologic properties of the storage formation and the confining units. Recognizing the importance of seal permeability for pressure buildup in semi-closed formations (Section 3), we consider seal permeability as one of the key parameters affecting the lateral and vertical volume affected by pressure buildup.

Notice that the simulation study involves an idealized multilayer aquifer-aquitard sequence at depth (from about 1,000 m to about 1600 m below surface); we have not yet modeled direct communication pathways with shallow aquifers and resulting environmental impact on groundwater resources. These topics will be addressed in future project phases, in conjunction with modeling of real-world storage sites.

4.1. Background on the Role of Seals and Seal Properties

Based on the results obtained for semi-closed systems (Section 3.4.4), we may expect seal permeability to be a significant factor also for pressure buildup and brine migration in laterally open formations. Suitable sites for long-term storage of CO_2 would typically have typically thick, laterally continuous shale, mudstone, or siltstone seals, i.e., sedimentary rocks formed by consolidation of clay and silt layers. Due to compaction, the sealing units have a lower porosity and permeability and a higher capillary entry pressure than the original clays and silts.

The primary role of the confining layers in CO_2 sequestration is to act as a permeability and capillary barrier to impede or prevent upward migration of supercritical CO_2. CO_2 tends to move upward because its density is smaller than that of water and native brine. The permeability of confining units is usually orders of magnitude lower than that of the target storage formation. As discussed in Section 3.2.2.3, seal permeability may vary in a wide range from approximately 10^{-16} to 10^{-23} m^2 (Neuzil, 1994; Hildenbrand et al, 2002, 2003; Hart et al., 2006). Capillarity also plays an important role in trapping CO_2 under a caprock unit because CO_2, as a non-wetting phase in a saline aquifer, can migrate into the seals only when the pressure buildup in the storage formation is higher than the capillary entry pressure in a CO_2-brine system. The capillary-barrier role of the confining units depends on the contrast of the pressure buildup in the storage formation and the entry pressure of the seals. Confining layers may have a wide range of entry pressures, as measured through laboratory CO_2-breakthrough experiments (Hildenbrand et al., 2002, 2003; Li et al., 2005). For example, Hildenbrand et al. (2002, 2003) reported capillary displacement pressure for CO_2-brine systems varying from 1 bar to 49 bar. A value of 210 bar was observed for Mississippian-age Midale Evaporite in the Weyburn Field in southeastern Saskatchewan, Canada (Li et al., 2005). The small permeability and high capillarity of confining units limit the leakage of CO_2 in its phase to a very small amount provided that there are no fractures and fault zones within the confining units.

Of course, the confining units also play a role in limiting the flow of native brine out of the storage formation into overlying and underlying strata. In contrast to CO_2 supercritical, this process is limited only by the small seal permeability; capillary sealing is not a limiting factor for brine leakage. Note that brine leakage may occur anywhere in the storage formation where pressure increases in response to CO_2 injection. Thus brine leakage can occur over a large area, considering that a pressure pulse can propagate far away from the injection zone. In comparison, the typical thickness of storage formation may be on the order of tens of meters, which implies that the area for lateral flow of displaced brine is orders of magnitude smaller than that for vertical flow. On the other

hand, the typical permeability within a storage formation is orders of magnitude larger than the typical permeability of a sealing unit.

How far the pressure buildup will extend into the lateral and the vertical direction depends on the competition between flow of displaced brine within the storage formation and inter-layer flow into over- and underlying units. In other words, if brine leakage out of the formation is important, the lateral displacement of brine within the formation becomes less extensive, and vice versa. Both lateral and vertical displacement need to be evaluated with respect to the possible environmental impact on shallow groundwater. For very small seal permeabilities, the native brine displaced by injected CO_2 will migrate mostly within the storage formation, which could affect freshwater resources located further updip (Figure 1) (Nicot, 2006). On the other hand, if the confining units have a relatively higher permeability, native brine may slowly migrate into and through the seals into neighboring formations, and may reach USDWs in extreme cases. At the same time, such considerable leakage would attenuate pressure buildup in the storage formation.

To our knowledge, no research has been conducted to date to systematically estimate the area of influence (with respect to brine migration and pressure buildup) in multilayer systems where lateral and vertical brine flow may compete. Our research therefore aims at (1) developing a basic understanding of the flow and pressure conditions in an open storage formation embedded in a sandstone/shale sequence, (2) exploring effects of interlayer communication through low-permeability seals and impact on lateral/vertical displacement, and (3) determining the region of influence as a function of formation/seal key properties.

4.2. Model Setup and Parameters

To understand pressure buildup and brine migration in open aquifers, we developed a numerical model simulating the multiphase flow and multicomponent transport of CO_2 and brine in a hypothetical multilayer formation, using the TOUGH2/ECO2N simulator (Pruess et al., 1999; Pruess, 2005). The transient pressure buildup, spatial CO_2 plume evolution, as well as brine flow and transport were simulated for various sensitivity cases. Results are presented as a function of time starting from the onset of injection and distance from the injection zone.

4.2.1. Model Setup

A two-dimensional radially symmetric model domain was chosen representing a deep saline aquifer with a typical sandstone/shale stratigraphy. The storage formation is 60 m thick and located at a depth of approximately 1,300 m (top of formation) below the ground surface. The storage formation is bounded at the top by a sealing unit of 100 m thickness each, followed by another 60 m thick aquifer and another 100 m thick shale formation (see Figure 12). The same sequence of shale/sandstone/shale underlies the storage formation. Altogether, the model domain includes three aquifers and four shales, with vertical depth ranging from 1,040 m to 1,620 m. Both the top and bottom model boundaries have fixed pressure boundary conditions set to the initial hydrostatic pressure value, meaning that fluids can freely flow into the over- and underlying aquifers. The outer lateral boundary is also open for fluids to escape from the model domain, again by imposing a fixed pressure conditions equal to hydrostatic. The lateral extent of the model domain was set to 200 km, which corresponds to a footprint area of more than 125,000 km^2. The large lateral extent was chosen to ensure that the boundary condition would have minimal effect on the simulation results.

CO_2 is injected in a zone of 125 m thickness and 50 m radial extent, representing not a single well, but rather a few distributed wells. Injection occurs over 30 years at an annual rate of 1.52 million tonnes of CO_2. The simulations continue for a 70-year post-injection

period. The aquifer is initially fully brine-saturated, assuming a hydrostatic fluid pressure distribution in the vertical direction. Isothermal conditions are modeled with a uniform temperature of 45ºC. The initial brine salinity is 0.15 (mass fraction).

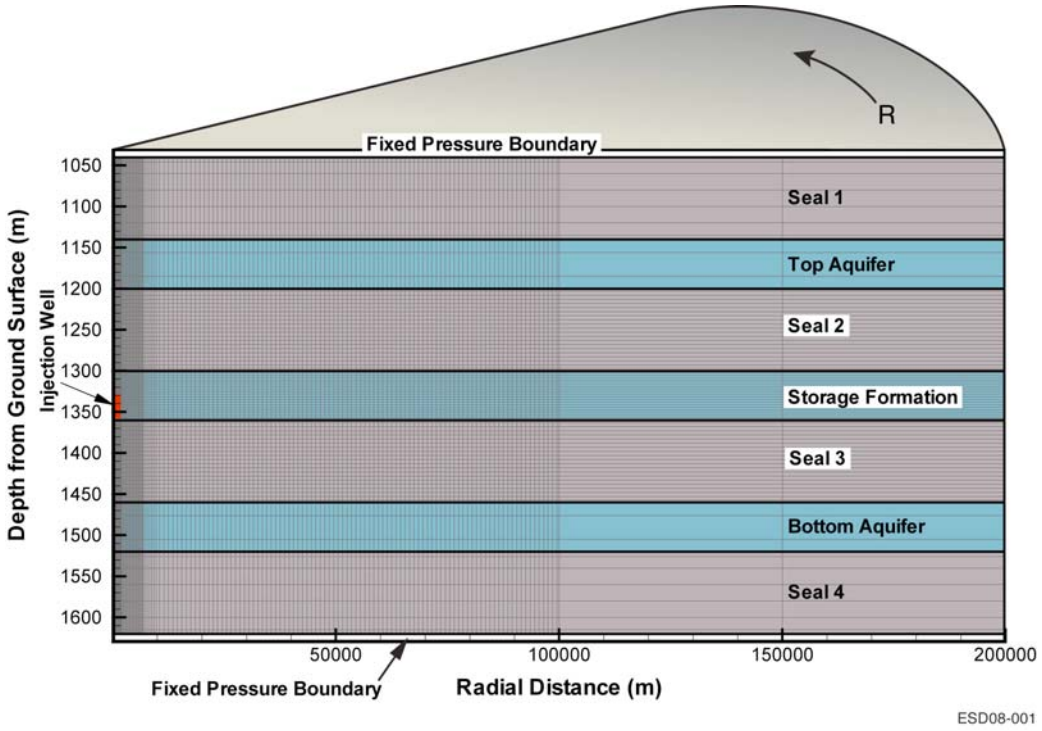

Figure 12. Schematic showing vertical cross section of radially symmetric model domain with deep brine formation for CO_2 storage and overlying/underlying sandstone/shale sequence. The numerical simulation grid is also depicted.

4.2.2. Model Parameters

The hydrogeologic properties chosen for the aquifer-seal sequence are given in Table 5. The properties of all three aquifers are typical of a sandstone brine formation suitable for CO_2 storage. Aquifer permeability and pore compressibility have been varied in sensitivity cases (Table 6). The properties of all four seals are representative of shale formations suitable for trapping CO_2, with lower permeability and higher compressibility compared to the sandstone. Seal permeability and compressibility have been varied as well. Specifically, seal permeability was varied over a wide range, from 1.0×10^{-16} to 1.0×10^{-21} m^2 plus one case with an impermeable seal (Table 6). Notice the differences in

sandstone and shale properties, for permeability (much lower in shale), compressibility (higher in shale), porosity (lower in shale), and van Genuchten (1980) α value (representing roughly the inverse of entry pressure for the nonwetting phase, higher entry pressure in shale). See a discussion of typical parameter ranges for storage formations and seals in Section 3.2.2.

Table 5. Typical values of hydrogeologic properties for the aquifer-seal system used in the simulations

Properties	**Values for Aquifers**	**Values for Seals**
Permeability (m^2)	1.0×10^{-13}	1.0×10^{-16} to 1.0×10^{-21}, and 0
Pore Compressibility (Pa^{-1})	4.5×10^{-10}	9.0×10^{-10}
Porosity	0.20	0.05
Van Genuchten m	0.46	0.46
Van Genuchten α (Pa^{-1})	5.1×10^{-5}	1.67×10^{-6}
Residual CO_2 saturation	0.05	0.05
Residual water saturation	0.30	0.30

Table 6. Simulation cases

Cases	**Formation Permeability (m^2)**	**Formation Compressibility (Pa^{-1})**	**Seal Permeability (m^2)**	**Seal Compressibility (Pa^{-1})**
Base Cases with Varying Seal Permeability	1.0×10^{-13}	4.5×10^{-10}	1.0×10^{-16}	9.0×10^{-10}
	1.0×10^{-13}	4.5×10^{-10}	1.0×10^{-17}	9.0×10^{-10}
	1.0×10^{-13}	4.5×10^{-10}	1.0×10^{-18}	9.0×10^{-10}
	1.0×10^{-13}	4.5×10^{-10}	1.0×10^{-19}	9.0×10^{-10}
	1.0×10^{-13}	4.5×10^{-10}	1.0×10^{-20}	9.0×10^{-10}
	1.0×10^{-13}	4.5×10^{-10}	1.0×10^{-21}	9.0×10^{-10}
	1.0×10^{-13}	4.5×10^{-10}	0	0
Sensitivity to Formation Permeability	2.0×10^{-13}	4.5×10^{-10}	1.0×10^{-18}	9.0×10^{-10}
	0.5×10^{-13}	4.5×10^{-10}	1.0×10^{-18}	9.0×10^{-10}
Sensitivity to Compressibility (Formation and Seal)	1.0×10^{-13}	4.5×10^{-09}	1.0×10^{-18}	9.0×10^{-09}
	1.0×10^{-13}	4.5×10^{-11}	1.0×10^{-18}	9.0×10^{-11}

4.3. Simulation Results and Discussion

4.3.1. Pressure Buildup

We evaluate the pressure buildup in response to CO_2 injection at the end of the 30-year injection period. Contours of pressure buildup are shown in Figure 13 for the base-case runs with seal permeabilities of 10^{-17}, 10^{-18}, 10^{-19}, and 10^{-20} m^2. A cutoff value of 0.2 bar is set for the contours; in other words, pressure buildup less than 0.2 bar, or less than a 2 m increase in the groundwater elevation, is not shown. It is obvious that seal permeability has a strong effect on both vertical and lateral pressure propagation. The low-permeability case (10^{-20} m^2) shows a pressure increase of 0.2 bar extending almost 80 km laterally within the storage formation. This radial extent corresponds to an area of influence covering more than 20,000 km^2. (Instead of the horixontal stratigraphy assumed in our simulations, we may imagine a gently updipping formation which is used for water supply from shallow groundwater resources at 80 km distance. Ignoring the impact of vertical variations in salinity and compressibility, the shallow groundwater resource would then experience a water table change of about 2 m.) Vertically, the region of pressure buildup is constrained to the sealing units immediately adjacent to the storage formation.

With increasing seal permeability, a different behavior shows. The high-permeability case (10^{-17} m^2), for example, has a lateral area of influence within the storage formation extending to less than 35 km in radial direction, or about 3,000 km^2. Vertical leakage out of the storage formation is quite effective, as apparent from pressure increases extending all the way to the top and bottom model boundaries. The maximum pressure near the injection zone is also reduced compared to the cases with lower seal permeability. Clearly, brine leakage due to inter-layer communication has a strong attenuation effect on the pressure conditions within the storage formation. However, as the vertical extent of the elevated-pressure zone shows, the pressure buildup may possibly reach shallow aquifers in cases with comparably high seal permeability via vertical inter-layer

communication. While contorted by the vertical-to-horizontal scale ratio in Figure 13, the pressure contours show clearly the predominantly horizontal flow within the aquifers (vertical contours) versus the predominantly vertical flow within the seals (close-to-horizontal contours).

The evolution of pressure change in the storage formation experienced at different distances (10, 20, 50, and 100 km) from the injection zone is shown in Figure 14, for all seal-permeability cases ranging from zero to 10^{-16} m^2. The time period is from 0 to 100 years, which comprises the 30-year injection period and a 70-year post-injection period. The transient pressure buildup in the storage formation is significantly affected by both radial location and seal permeability. Pressure buildup is larger close to the injection zone; also the response time at the beginning and end of injection is shorter. Further away, the pressure response is weaker and occurs later. In fact, the maximum pressure is observed years to decades after injection stops when measured at 50 and 100 km radial extent. While strong dependence of pressure buildup on location is expected (in particular in a radial-symmetric setting), the significant impact of seal permeability may be surprising. We may group all cases with seal permeability equal to or lower than 10^{-20} m^2 into an "impermeable-seal" category; these cases all feature similar pressure transients showing the strongest pressure perturbation in the storage formation. Relative to this, all other cases show moderate to drastic pressure reduction, about 20% in the 10^{-19} m^2 case, about 50% in the 10^{-18} m^2, and about 80% in the 10^{-17} m^2 case, demonstrating again the importance of inter-layer brine flow of displaced brine. Almost no pressure buildup is observed in the 10^{-16} m^2 case, even at a close distance of 10 km to the injection zone. We caution, however, that the migration of buoyant CO_2 into the caprock is significant in this case, suggesting that the sealing characteristics would not allow for safe long-term trapping of CO_2.

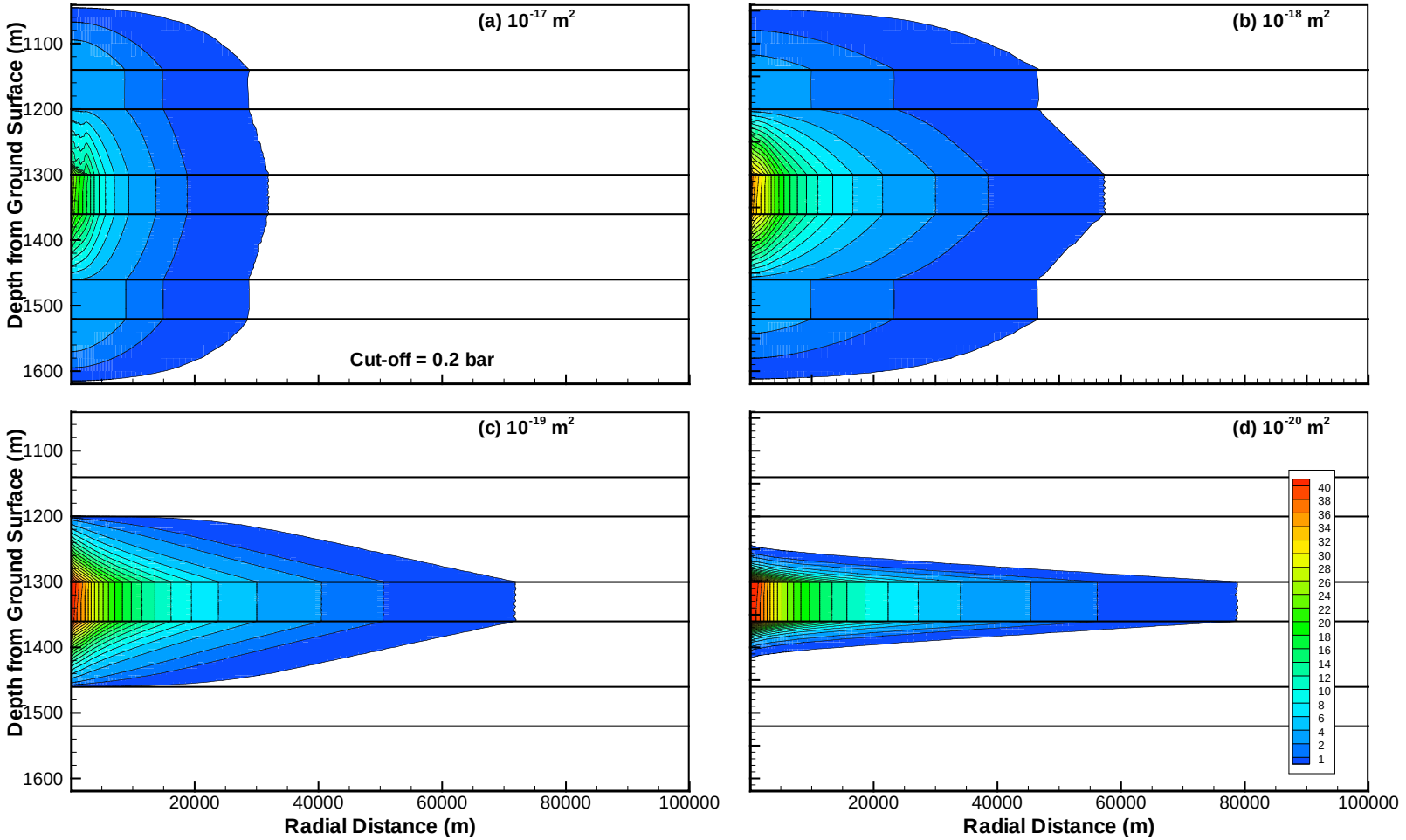

Figure 13. Spatial distribution of pressure buildup (change in fluid pressure from the initial hydrostatic condition), at 30 years of CO_2 injection, as a function of seal permeability

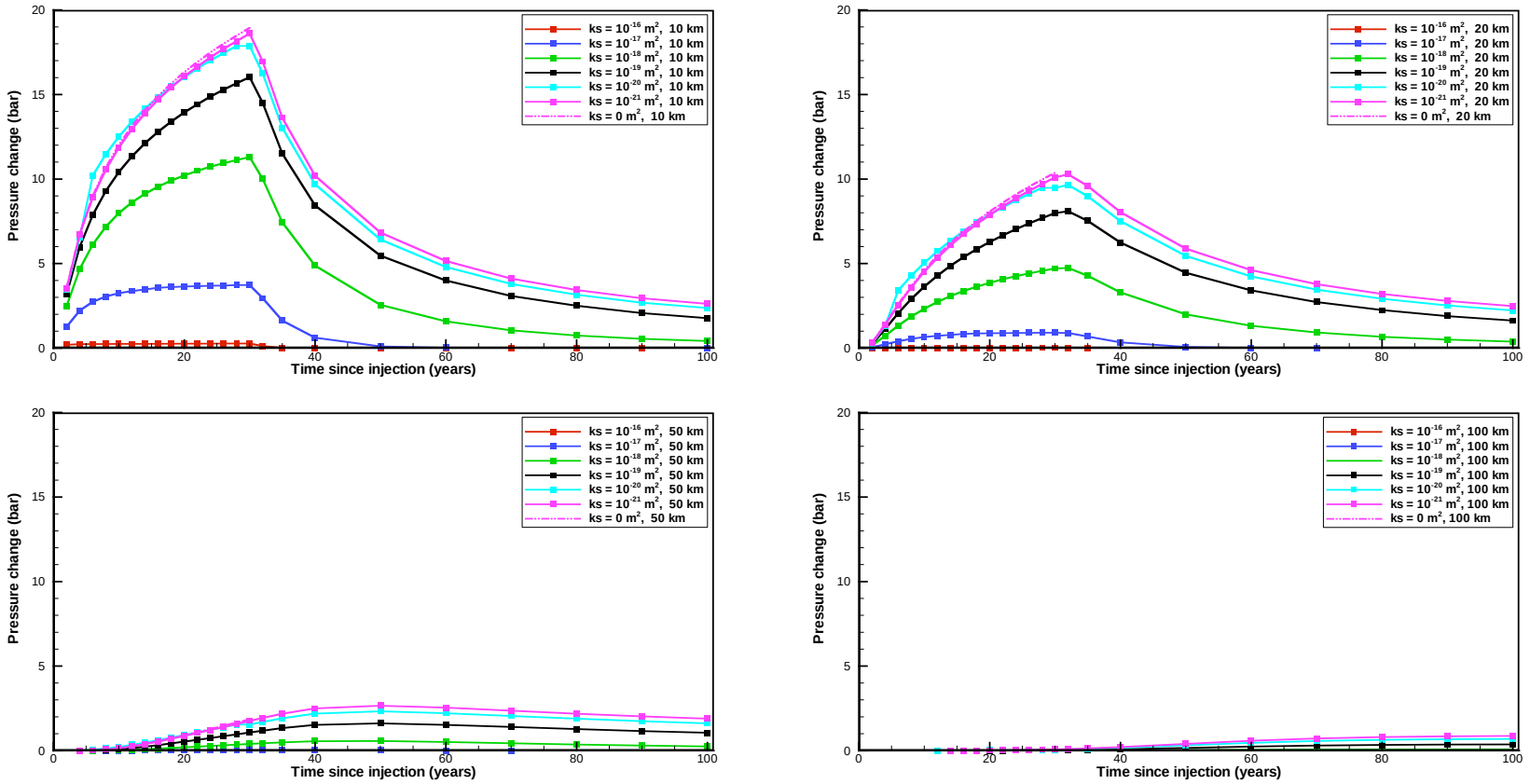

Figure 14. Sensitivity of pressure change to seal permeability, at different radial locations in the storage formation

The extremely large area of influence observed with respect to pressure buildup may have considerable implications for the storage capacity at a given site. To provide a perspective, we may assume that the storage formation shown in Figure 12 communicates with a valuable groundwater resource and that the pressure buildup observed in Figures 13 and 14 corresponds to a pressure threshold that should not be exceeded. We may then calculate the storage efficiency for these conditions, i.e., the volume of CO_2 stored divided by the total initial porosity of the formation. With total of CO_2 volume of about 65 million m^3 injected in our simulation example (30 years with 1.52 million tones annually, divided by a density of 0.7 tonnes/m^3), and using the total initial pore space for the 50-km radial domain as reference volume, the maximum storage efficiency as constrained by pressure buildup is less than 0.1%. This value is significantly smaller than the storage efficiency estimated in DOE (2007), where pressure constraints related to brine displacement are not considered (Section 3.5.5).

4.3.2. Spatial Distribution of CO_2 Plume

We use a 10^{-18}-m^2 seal permeability as a base case to discuss the evolution of the CO_2 plume during the injection period, shown in Figure 15 together with pressure buildup contours and brine flow vectors. Though the seal permeability is high enough to allow for inter-layer brine flow (see Figures 13 and 14), the CO_2 plume is safely trapped by permeability and capillary barriers. The plume is approximately 3 km wide and is concentrated at the top of the storage formation. The 3-km plume size compares to the approximately 60 km radial extent experiencing a pressure buildup of 0.2 bar or more (Figure 13). This difference in region of influence quantifies earlier discussion about the footprint area of the CO_2 plume typically much smaller than the footprint area of elevated pressure (Figure 1). The flow vectors indicate horizontal brine flow within the storage formation, with the exception of the plume area where buoyant CO_2 migration generates a downward component of brine flow. The vector length in Figure 15 corresponds to the magnitude of velocity, with the result that the low-velocity flow in the seals and top/bottom aquifers are too small to be visible. Notice that the CO_2 plumes are basically identical for all seal permeability cases, with the exception of the case with 10^{-16}-m^2 permeability (these cases are not shown here for brevity). As indicated before, CO_2 is not safely trapped in this case; the plume leaks into the caprock and almost reaches the overlying aquifer (top aquifer) after 30 years of injection.

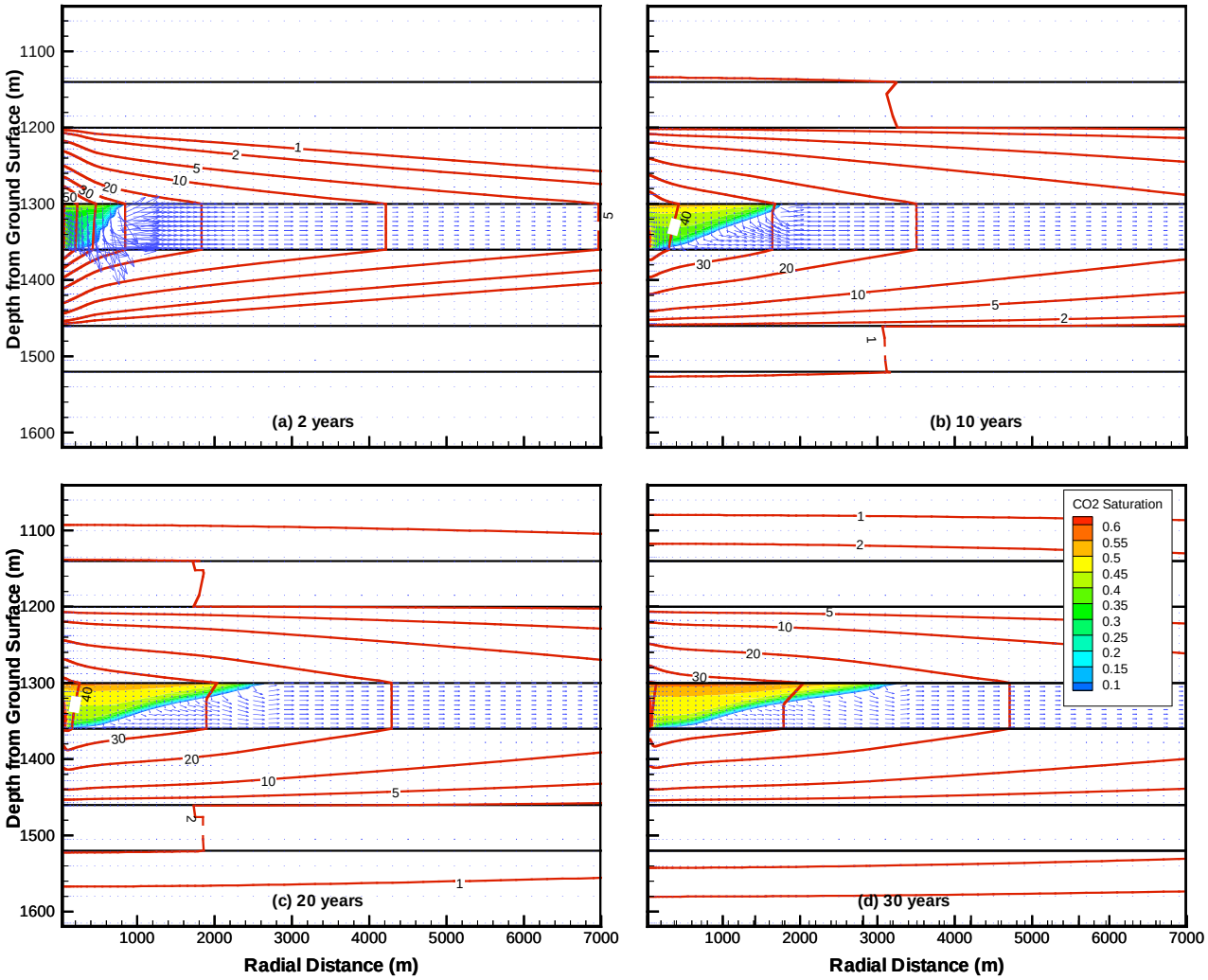

Figure 15. Contours of CO_2 saturation (flooded contours), contours of fluid pressure change (in red lines), and brine flow vectors for the case with a 10^{-18}-m^2 seal permeability

4.3.3. Characteristics of Brine Displacement

We discuss here the brine displacement/migration characteristics as a function of time, radial location, and seal permeability. Specifically, we evaluate the total volumetric brine flow at different radial cross-sections within the storage formation (Figure 16), the total volumetric inter-layer brine flow into different sandstone/shale units (Figure 17), and the lateral brine transport velocity within the storage formation (Figure 18).

For reference, the volumetric brine flow is compared in Figure 16 to the volumetric CO_2 injection rate, which is about 5,500 m^3 per day at storage conditions. Notice the modest changes in CO_2 injection rate, indicative of changes in pressure conditions (and related CO_2 density changes) during the injection period. (The plot shows the volumetric CO_2 injection rate for the sensitivity case wit a seal permeability of 10^{-18} m^2.) For a pure piston-type flow in the storage formation, i.e., without compressibility effects and assuming impermeable seals, the volumetric rate of brine displacement at any radial location would be approximately equal to the volumetric rate of CO_2 injection. The results in Figure 16 demonstrate, however, that both compressibility and brine leakage into non-ideal seals are important in reducing the brine flow rates in the storage formation to much less of the CO_2 injection rates. Compressibility is the dominant factor in the 10^{-21} m^2 and 10^{-20} m^2 sensitivity cases, in which brine leakage out of the storage formation is not significant. Since the effect of compressibility increases with the volume affected by pressure changes, the volumetric rate of brine displacement depends strongly on radial location. For example, the maximum brine flow rate through the lateral cross-section at 10 km (i.e., $A = 2\times\pi\times 60\ m\times 10\ km$) is about 5,000 m^3 per day, or about 90% of the volumetric CO_2 flow rate. The brine flow rate reduces to about 4,400 m^3 per day at 30 km, about 2,500 m^3 per day at 50 km, and about 800 m^3 per day at 100 km.

Brine leakage out of the formation into overlying/underlying units causes additional attenuation. For the case with a seal permeability of 10^{-18} m^2, the maximum brine flow

rate within the storage formation reduces to about 4,200 m^3 per day at 10 km, about 3,000 m^3 per day at 30 km, about 800 m^3 per day at 50 km, and about zero at 100 km. It becomes clear from these results that the impact of vertical inter-layer communication through the sealing units needs to be considered when estimating environmental issues related to pressure buildup and brine displacement. Our example results suggest that vertical brine leakage becomes important when the seal permeability is higher than about 10^{-20} m^2.

Figure 17 shows the evolution of the total volumetric inter-layer brine flow rate through different sandstone/shale interfaces (see Figure 12 for the schematic stratigraphy). Starting from the injection unit, vertical brine flow has been integrated over the interface between the storage formation and the overlying/underlying seals ("Seal 2 Bottom and Seal 3 Top"), the interface between these seals and the overlying/underlying aquifers ("Seal 2 Top and Seal 3 Bottom"), the interface between these aquifers and the overlying/underlying seals ("Seal 1 Bottom and Seal 4 Top"), and finally the interface between the top/bottom seals and the model boundaries ("Seal 1 Top and Seal 4 Bottom"). Depending on the seal permeability case, brine leakage out of the storage formation could be dominant (i.e., more than 90% of the volumetric CO_2 injection rate for seal permeability equal to a larger than 10^{-17} m^2), but this leakage rate reduces with increasing vertical distance, indicating the attenuation capacity of the overlying/underlying aquifers and aquitards. Displaced brine escapes from the model domain through the top/bottom boundary in the three sensitivity cases with relatively high seal permeabilities of 10^{-16} m^2, 10^{-17} m^2, and 10^{-18} m^2. It should be evaluated in such cases whether pressure changes and brine displacement could propagate through the entire vertical strata all the way to shallow groundwater resources. From extrapolation of the brine flows observed in Figure 17 (with the top boundary at 1,040 m below ground surface), it seems rather unlikely that groundwater resources near the ground surface should be affected in any of the simulation cases.

In saturated porous media, the pressure pulse generated in the injection zone propagates much faster and much further than the actual movement of a fluid particle. To evaluate the possible displacement of a particle dissolved in the native brine, we have plotted in Figure 18 the particle transport velocity in the storage formation, as a function of time for different radial locations and different seal permeability cases. For comparison, we first calculate the maximum possible transport velocity assuming a pure piston-type displacement flow in the storage formation. Because the model domain is radial-symmetric, a uniform volumetric flux equal to the injection rate of CO_2 corresponds to velocity values decreasing with radial distance. The piston-type transport velocities can be easily calculated as about 2.7 m per year at 10 km, 1.3 per year at 30 km, 0.5 m per year at 50 km, and 0.25 m per year at 100 km.

To put these numbers into perspective, the regional Darcy velocity in the Alberta Basin is 0.01 to 0.1 m per year, which translates to a transport velocity of 0.1 to 1 m per year (assuming an effective porosity of 0.1) (Bachu et al., 1994). In other words, even the upper bounding limits provided by the piston-flow estimates are not excessively large compared to the natural groundwater velocities in deep basins. Furthermore, the transport velocities observed in Figure 18 are similar to the piston-flow estimates only for small radii and small seal permeabilities. In all other cases, compressibility and/or brine leakage into non-ideal seals reduce the actual transport velocities to a fraction of the piston-flow estimates. In conclusion, although the region of influence is very large with respect to pressure changes, the actual brine displacement velocities are quite small compared to natural groundwater flows, and the travel distance of a particle dissolved in the brine would be rather insignificant. As an example, assuming a constant upper-limit transport velocity of 2.7 m per day, a particle would migrate about 100 m during the injection period. It appears that environmental impacts related to updip displacement of saline or brackish water should be small, at least in settings where radial-symmetric flow is a reasonable approximation.

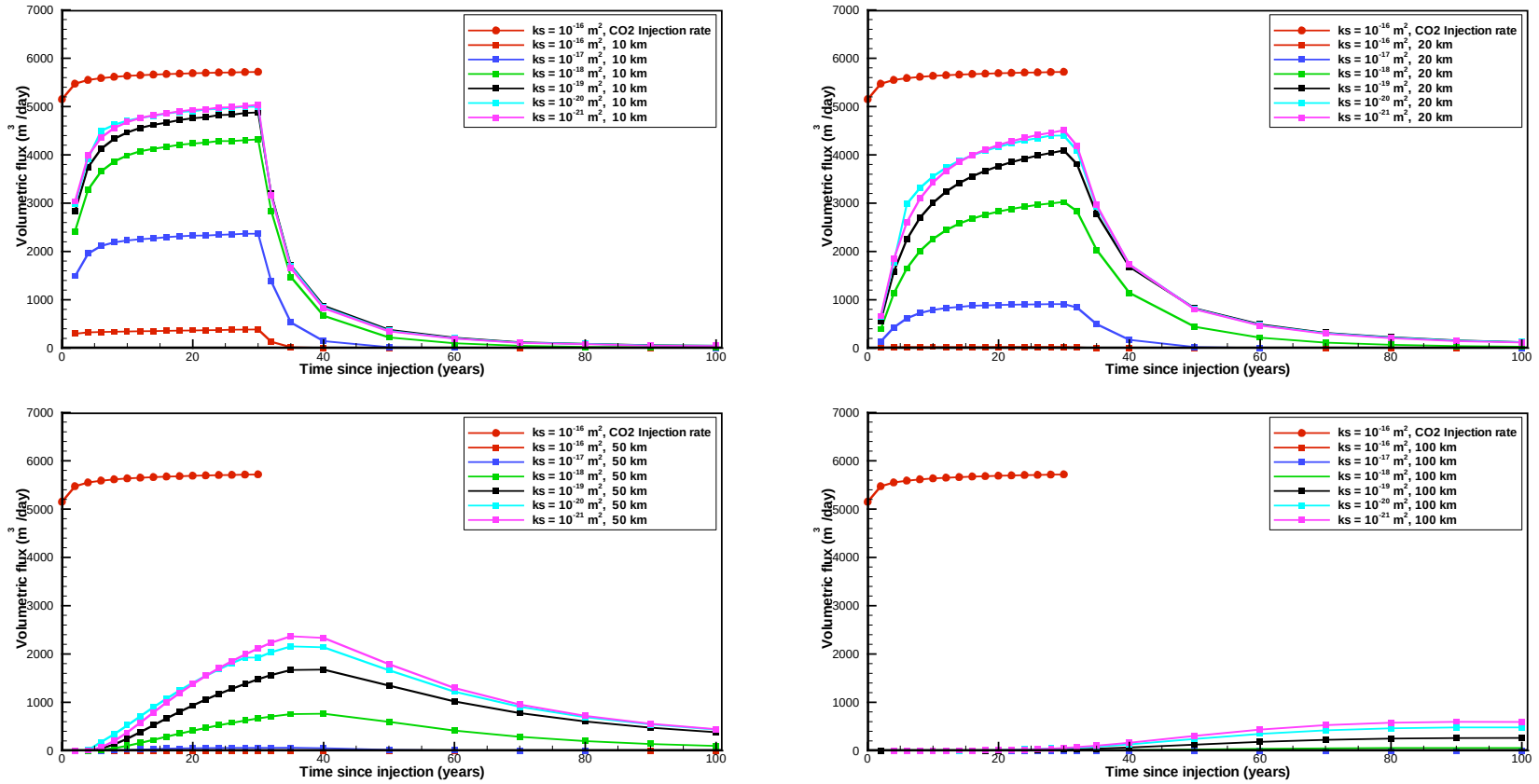

Figure 16. Evolution of total volumetric brine flow rate in the storage formation, for different seal permeabilities and radial locations. The brine flow rate is integrated over the entire cross-sectional (radial-symmetric) interface at a given location in the storage formation.

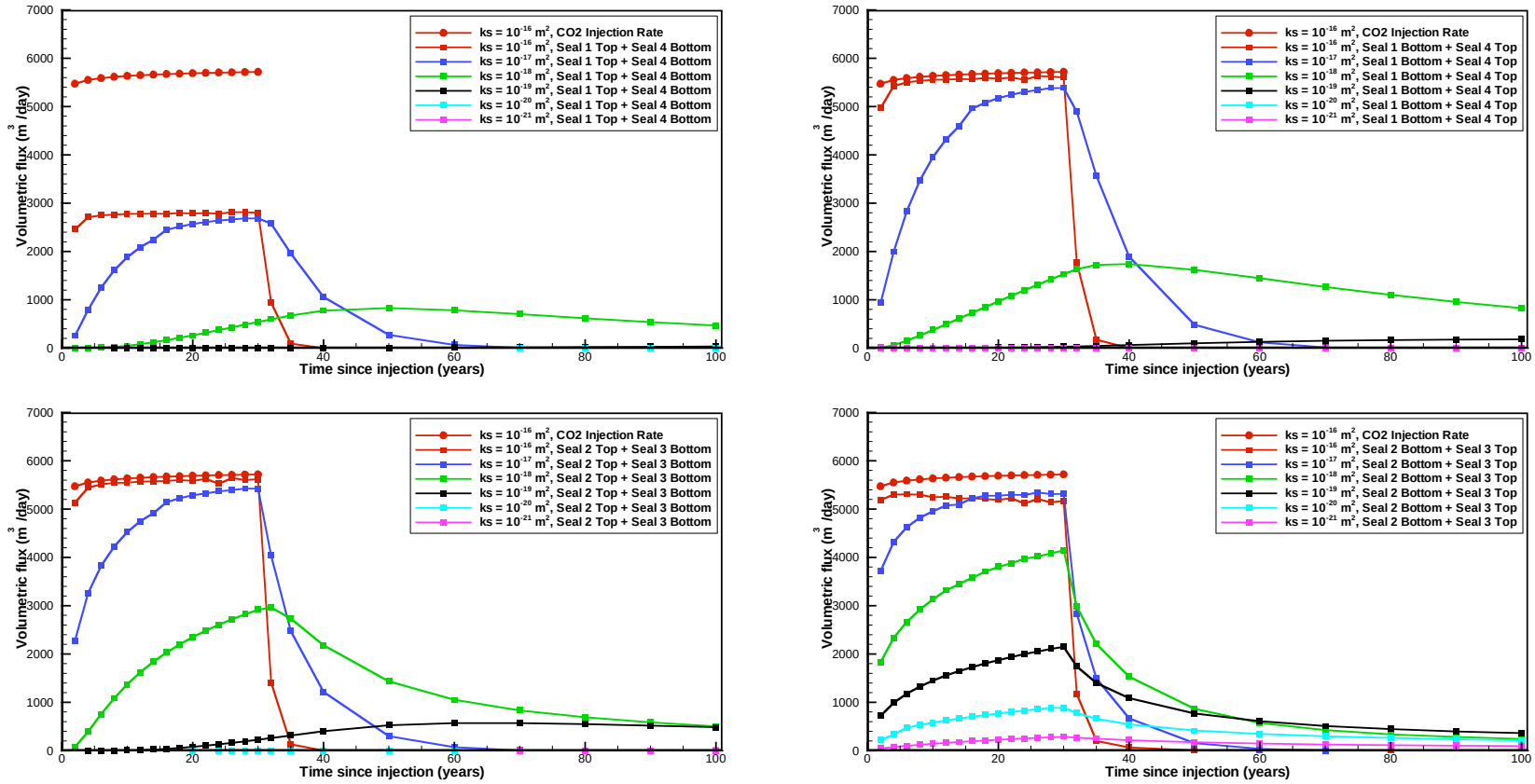

Figure 17. Evolution of total volumetric brine flow rate through different sandstone/shale interfaces, for different seal permeabilities. Starting from the injection unit, vertical brine flow has been integrated over the interface between the storage formation and the overlying/ underlying seals “Seal 2 Bottom and Seal 3 Top”, the interface between these seals and the overlying/underlying aquifers “Seal 2 Top and Seal 3 Bottom”, the interface between these aquifers and the overlying/underlying seals “Seal 1 Bottom and Seal 4 Top”, and finally the interface between the top/bottom seals and the model boundaries “Seal 1 Top and Seal 4 Bottom”.

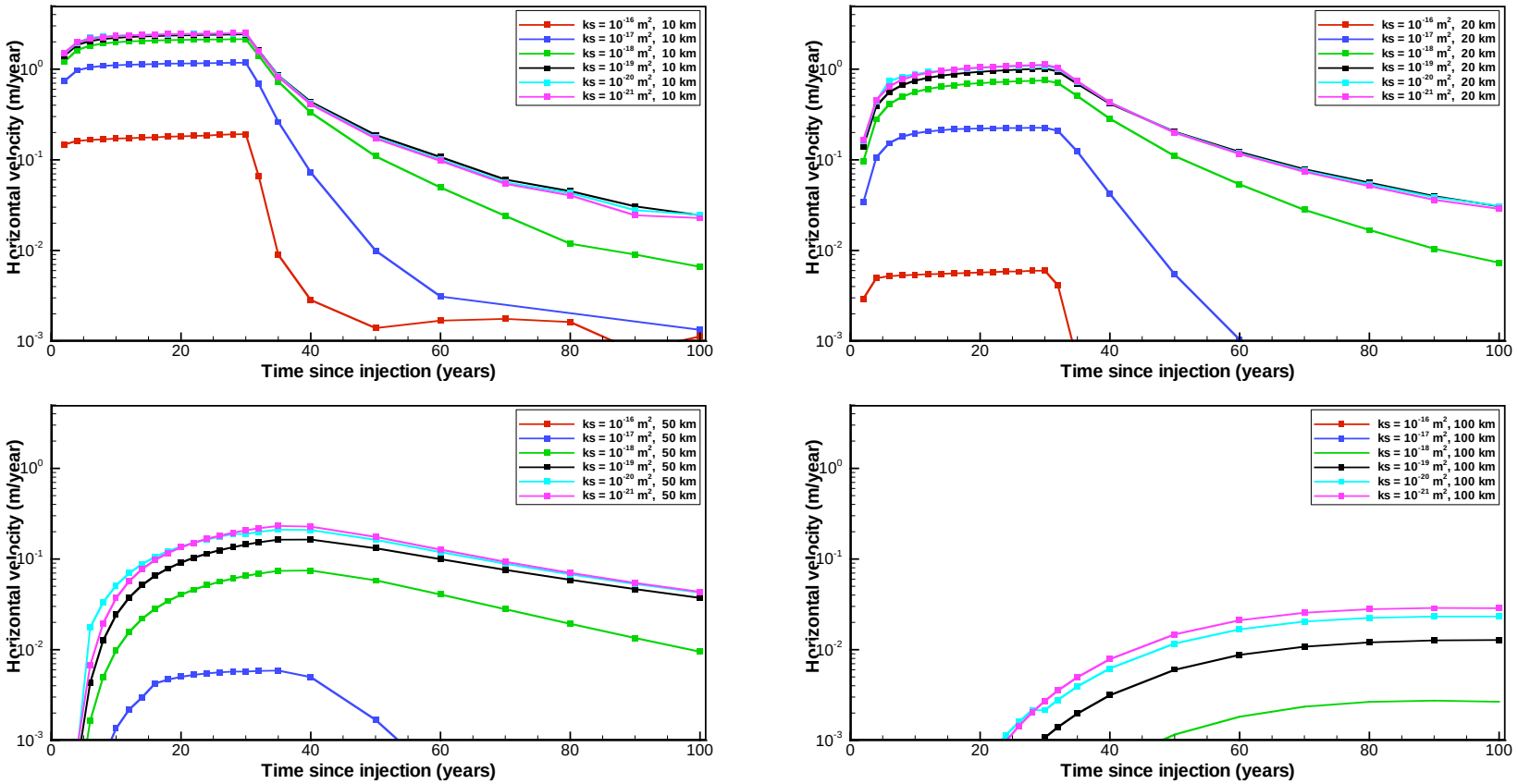

Figure 18. Evolution of lateral transport velocity of displaced brine in the storage formation, for different seal permeabilities and radial locations.

4.3.4. Further Sensitivities

In previous sections, we have established the need for considering the multilayer seal characteristics (i.e., seal permeability) when analyzing the pressure buildup and brine displacement characteristics in a storage formation. Here, we evaluate sensitivity to other key properties, namely the permeability of the storage formation and the pore compressibility of the sandstone/shale sequence. Using the base case with a seal permeability of 10^{-18} m^2 as a starting point, the following sensitivity cases were conducted: (1) increase of storage formation permeability by a factor of two, (2) reduction of storage formation permeability by a factor of two, (3) increase in pore compressibility by a factor of ten, and (4) reduction in pore compressibility by a factor of ten. Results are depicted in Figure 19, showing pressure evolution (top) and total volumetric brine flow (bottom) in the storage formation at radial extents of 10 and 20 km, for the different sensitivity cases and an injection period of 30 years.

Both parameters, permeability and compressibility, significantly affect both the storage formation conditions and the inter-layer leakage into neighboring units. A decrease in reservoir permeability, for example, results in a slightly delayed, but ultimately stronger pressure buildup in the storage formation, because of less brine flow in lateral direction (Figure 19a). As a result of the increasing pressure buildup in the storage formation, the inter-layer leakage of brine into overlying and underlying units increases compared to the base case, while the total volumetric brine flow within the storage formation reduces significantly, leading to smaller pressure buildup further away from the injection zone (Figure 19b). An increase in pore compressibility causes reduction in both pressure buildup and horizontal brine flux in the storage formation (Figure 19c,d). A higher compressibility means that more fluid volume can be stored in the porous formation in response to a given pressure change. As a result, less pressure buildup is generated from CO_2 injection and less brine is being displaced at a given radial location in the storage formation.

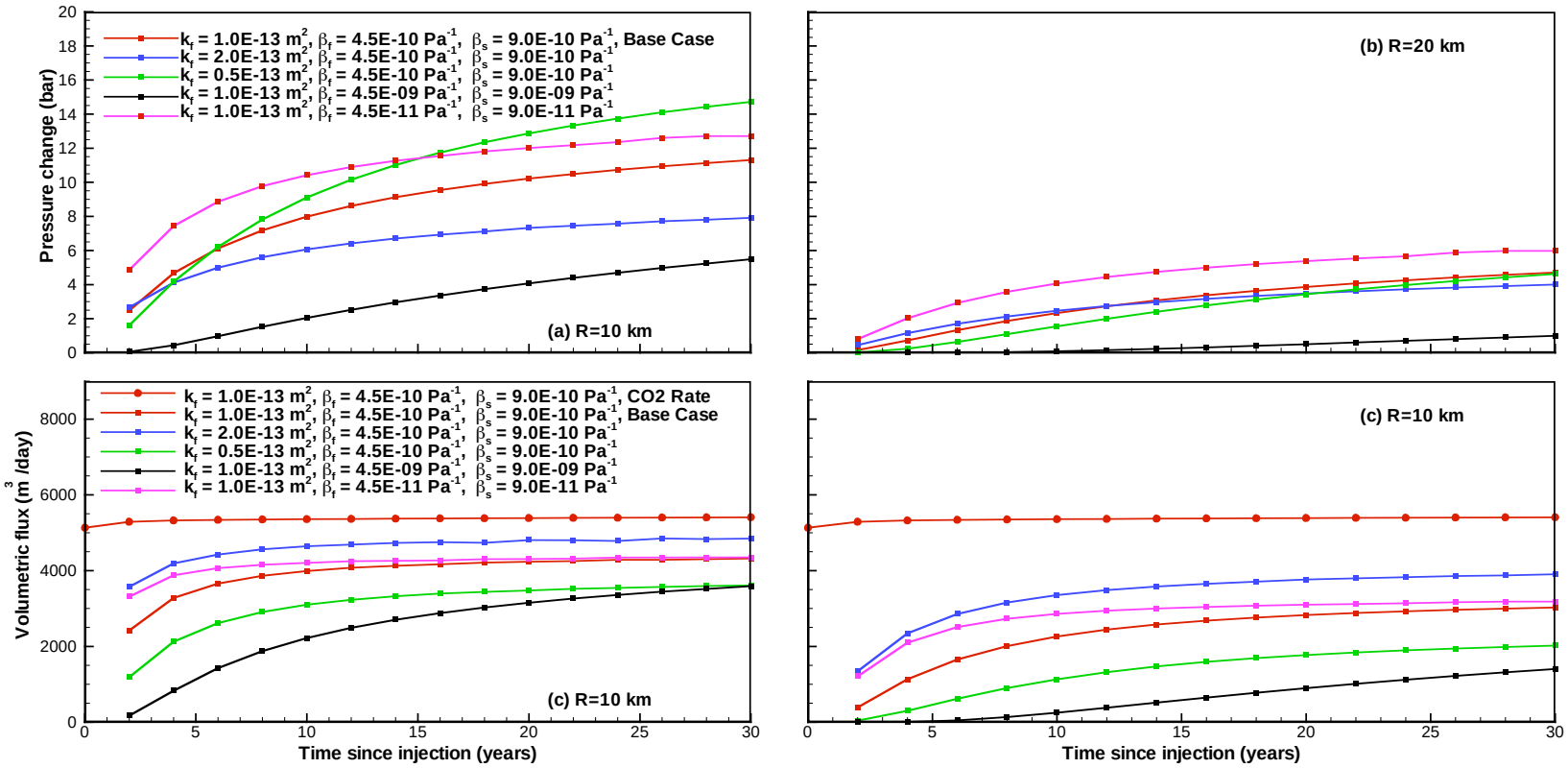

Figure 19. Evolution of pressure buildup change (top) and total volumetric brine flow rate in the storage formation (bottom), for different sensitivity cases of storage formation permeability and pore compressibility.

4.4. Summary for Open Multilayer Systems

1) With respect to pressure changes in the storage formation, the region of influence in response to CO_2 injection can be extremely large. For the radial-symmetric domain evaluated in this study, considerable pressure buildup was observed 100 km away from the injection zone (up to one bar for certain sensitivity cases). Such pressure changes may cause problems if experienced in near-surface groundwater systems, a possible concern in a storage formation that extends updip to form a freshwater resource (one bar translates to a water table change of 10 m). The extremely large area of influence observed with respect to pressure buildup may have important implications for the maximum CO_2 storage capacity at a given site.

2) While the pressure pulse travels fast and far within the storage formation, the lateral brine flow velocities are quite small, not much larger than those of natural groundwater flows in deep basins. The migration distance of a particle dissolved in brine (at a location not too close to the injection zone) is only a few hundred meters or less for a time period of 100 years during and after injection. This is indicative, for example, of the possible migration of the 10,000 mg/L TDS iso-concentration line that defines whether a groundwater can be considered an underground source of drinking water (USDWs). We caution that these results have been obtained for a radial-symmetric system, which is a reasonable approximation for a single-source injection site.

3) Characteristics of pressure buildup and brine displacement are sensitive to key properties of the storage formation (e.g., lateral permeability, pore compressibility), which is not surprising. However, they are also strongly affected by the properties of the multilayer sandstone/shale units overlying and underlying the storage formation, which is somewhat surprising. Seals that are suitable for long-term trapping of CO_2 allow for considerable brine leakage out of the formation vertically upward and downward. As a result, the pressure buildup and lateral flow in the storage formation

is moderately to strongly reduced compared to a perfect seal with zero or close-to-zero permeability. It is important to fully understand the multilayer characteristics of a storage site if the large-scale brine displacement resulting from CO_2 injection, and the possible environmental impacts on USDWs, are to be investigated.

4) Our simulation example involved an idealized multilayer sequence at depth (from about 1,000 m to about 1600 m below surface); direct communication pathways with shallow aquifers and resulting environmental impact on groundwater resources have not been modeled explicitly. These topics will be addressed in future project phases, in conjunction with modeling of real-world storage sites (see Section 5).

5) The example simulations presented are associated with the injection and storage of 1.5 million tones of CO_2 per year originating from one major CO_2 point source. When more than one large point source would store CO_2 within a sedimentary basin, their regions of elevated pressure may be interacting and overlapping, leading to different and possibly stronger environmental impacts. Multiple-source scenarios will be studied in future project phases, possibly in conjunction with modeling of the Mount Simon sandstone (Section 5).

6) Related research results are being published in Tsang et al. (2007) and Birkholzer et al. (in preparation), see Section 8.

5. Future Work

5.1. Hydromechanical Simulations

One of the future project tasks outlined in Section 2 is to evaluate hydromechanical aspects of CO2 injection that could potentially affect the expected pressure buildup and brine migration characteristics. Geomechanical modeling will be conducted using the coupled reservoir-geomechanical simulator TOUGH-FLAC, which is described in detail in Rutqvist et al. (2002). In preparation of this future project phase, TOUGH-FLAC has recently been enhanced to study the coupled multi-phase flow and geomechanical conditions associated with underground injection of CO_2. Example applications include evaluation of tensile and shear failure in response to CO_2 storage in a multilayered geological system (Rutqvist et al., 2007a) and simulation of fault-slip behavior for a discrete fault in a aquifer-caprock system (Figure 20) (Rutqvist et al., 2007b).

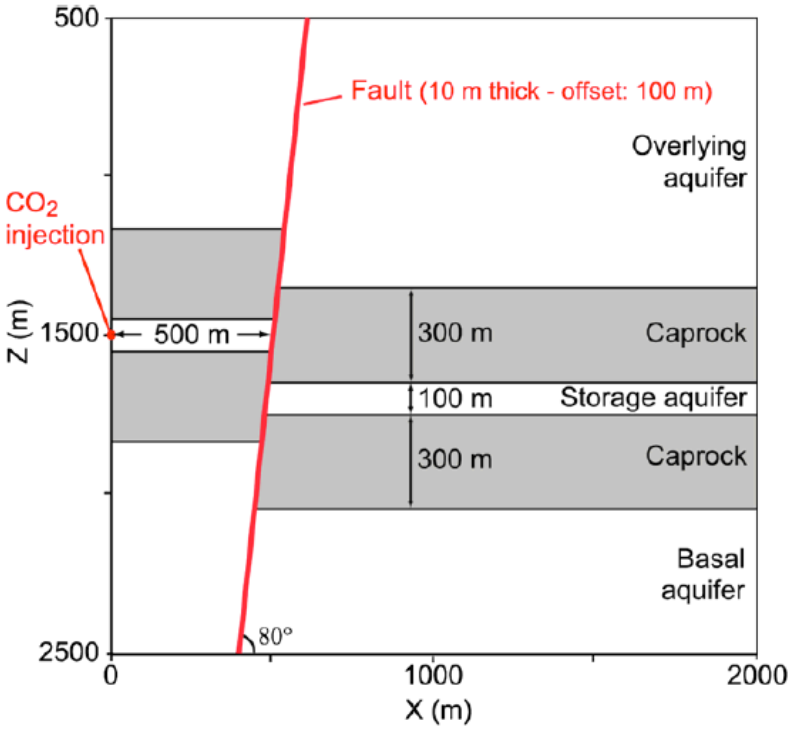

Figure 20. Schematic setup for fault-slip analysis of discrete fault hydromechanical behavior during CO_2 injection (Rutqvist et al., 2007a)

5.2. Modeling of Regional Groundwater Systems

5.2.1. Possible Sites

Two large basins, the Illinois Basin and Sacramento Basin, have been tentatively selected as candidate sites for regional-scale modeling of groundwater systems in response to CO_2 storage. These basins were selected for three main reasons. (1) They are located in regions with a large portfolio of existing and potential future point sources. (2) They contain formations potentially suitable for sequestering large volumes of CO_2. (3) They contain a variety of inter- and intra-basin hydrogeological conditions, some subset of which is likely to be encountered at most high-capacity sequestration sites.

Both basins contain thick, regionally extensive permeable formations. The conditions in the Illinois Basin are representative of less faulted and folded formations. In contrast, the Sacramento Basin contains a range of intra-basin structures likely representative of structurally complex, compartmentalized, and extensively faulted formations. A short description of these two basins follows.

Illinois Basin

The Illinois Basin encompasses most of Illinois, along with southwestern Indiana, and western Kentucky. The Midwest Geological Partnership Consortium (MGSC) views the Mount Simon Sandstone as a primary target for CO_2 storage (MGSC 2005). The Mount Simon is a deep saline formation of regional extent with proven seals and large storage potential. While offering a large storage capacity, the Mount Simon is expected to be used at multiple sequestration sites, based on the current portfolio of industrial point sources and the predicted future developments. The following discussion of the Mount Simon Sandstone is primarily from MGSC (2005).

As shown in Figure 21, the Mount Simon Sandstone ranges up to greater than 600 meters (2,000 feet) thick in the northern part of the Illinois Basin. Dipping south, the top of the Mount Simon Sandstone is less than 600 meters (-2000 feet) below mean sea level (msl)

just north of the basin and greater than -3,700 meters (-12,000 feet) below msl in the southern portion of the basin (Figure 22). The Mount Simon Sandstone grades updip into a freshwater aquifer in Wisconsin (over the Wisconsin Arch to the north of the Illinois Basin). Thus there is concern about potential degradation of freshwater resources due to brine displacement resulting from CO_2 sequestration in the Mount Simon Sandstone to the south.

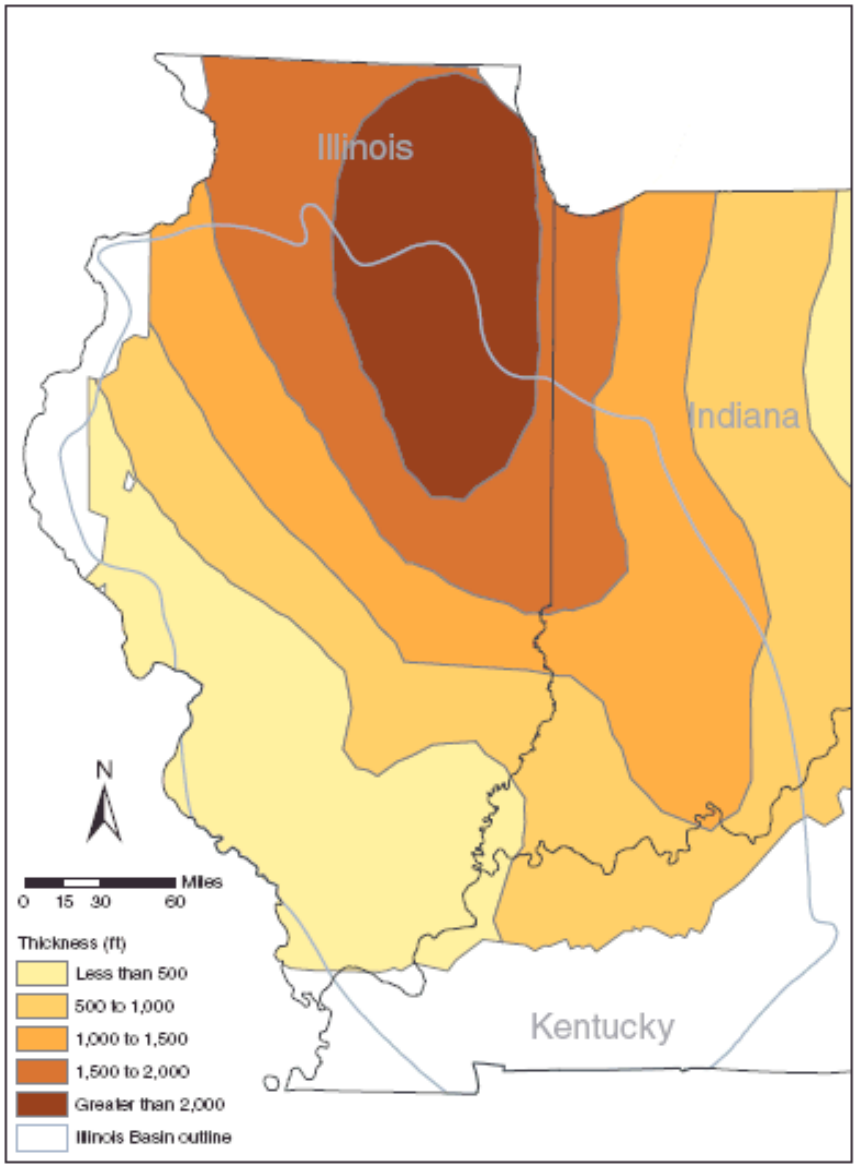

Figure 21. Contour map of the thickness of the Cambrian Mt. Simon Sandstone within the Illinois Basin (from MGSC 2005)

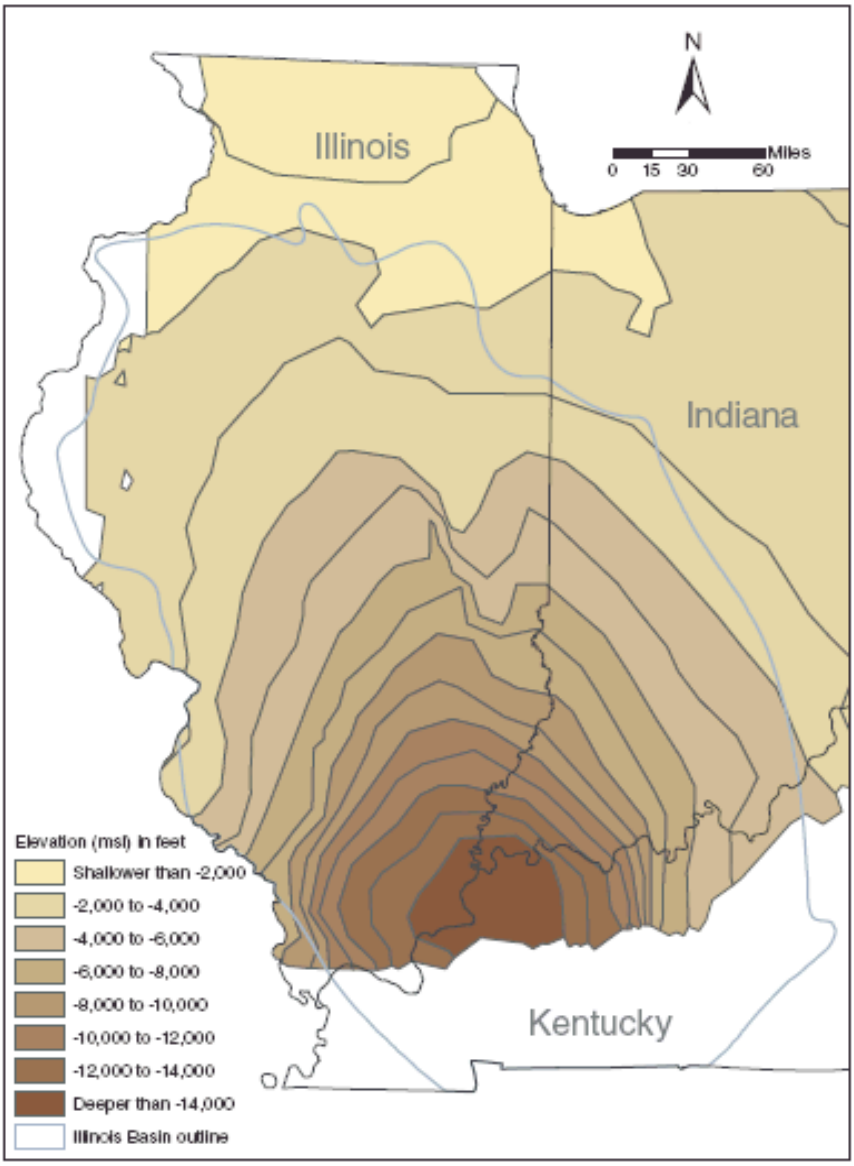

Figure 22. Structure on top of the Mt. Simon Sandstone within the Illinois Basin (from MGSC 2005)

Besides the open, updip boundary condition into fresh groundwater to the north, the Mount Simon Sandstone in the Illinois Basin includes a suite of other boundary conditions in the remaining directions. To the southwest it pinches out at depth against the Ozark Dome. Downdip to the south, it is likely cut by the east-west trending Cottage Grove Fault System in Illinois and the Rough Creek Graben in Indiana. A relative lack

of hydrocarbon resources at and south of Cottage Grove Fault System strongly suggests these faults are conductive on geologic time scales. The Mount Simon Sandstone extends to the east across the Cincinnati Arch into the western portion of the Appalachian Basin, and northeast across the Kankakee Arch into the Michigan Basin (MRCSP 2005).

The sealing layer over the Mount Simon Sandstone is the Eau Claire Formation. This Formation consists of siltstone and shale in the center of the Illinois Basin, but grades to dolomitic sandstone and sandy dolomite updip to the north, and predominantly dolomite and limestone downdip to the south. Therefore the sealing quality of the Eau Claire Formation varies with higher potential for fluid flow through the seal away from the central portion of the Illinois Basin.

In sum, study of induced brine flow and pressure changes in the Mount Simon Sandstone in the Illinois Basin will address a number of potentially relevant, basin-scale hydrogeologic conditions, including updip impacts to groundwater resources, interbasin effects, and interaction with potentially permeable faults.

Sacramento Basin

The Sacramento Basin underlies the northern half of the Great Valley of California. The basin is bounded to the west by the Coast Ranges, to the north by the Klamath Mountains, to the east by the Cascade and Sierra Nevada (Magoon and Valin, 1995), and to the south by the Stockton Arch (WESTCARB 2005). The Sacramento Basin is one of the six "most promising" basins for CO_2 storage in California (WESTCARB 2005). The remainder of this discussion is based primarily on WESTCARB (2005).

The focus of the brine displacement study will be the Mokelumne River Formation in the Sacramento Basin (Figures 23 and 24). This formation is part of the marine shelf deposits shed primarily from the Sierran volcanic arc in the Cretaceous. Subsequent uplift of the Coast Ranges bounded the asymmetric Sacramento Basin to the west. The

synclinal axis of this basin is significantly to the west of its geometric midline as shown on Figure 23 modified from CDOG (1982).

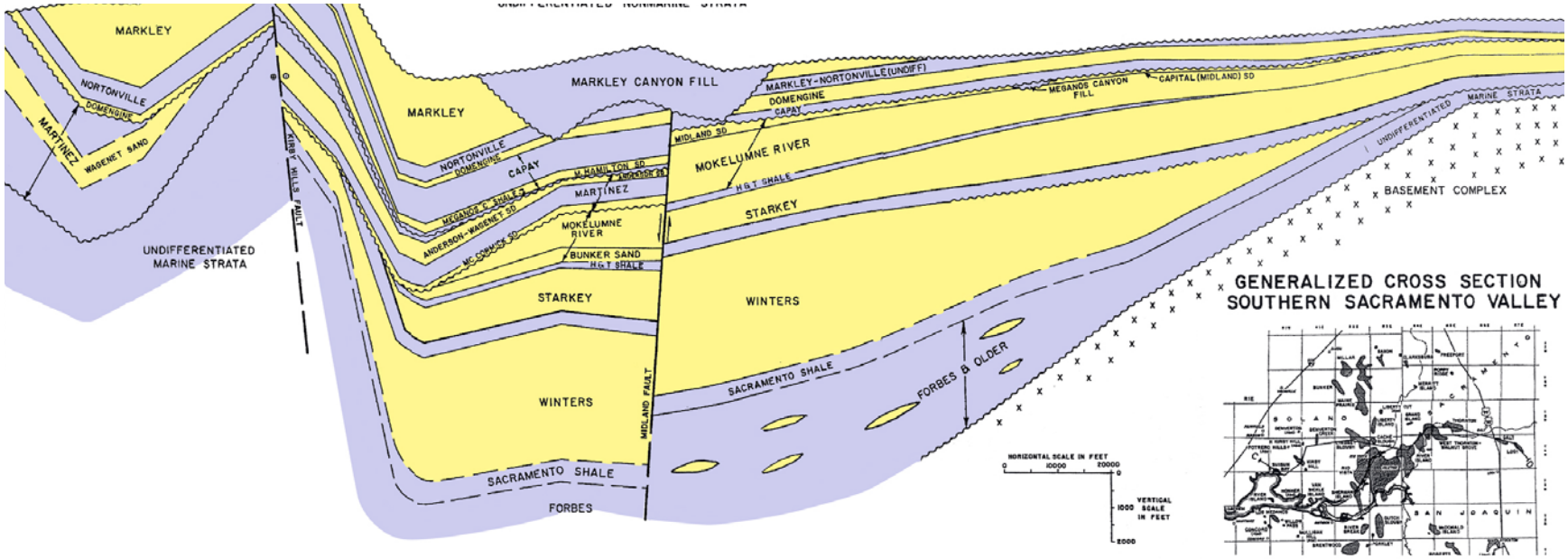

Figure 23. Generalized Cross-Section of Southern Sacramento Valley (colorized from CDOG 1982)

Depths to the Mokelumne River Formation range from less than 600 meters (2,000 feet) in the northern portion of the basin to 2,700 meters (9,000 feet) in the southern portion of the basin. The net thickness of these sands ranges up to 700 meters (2,250 feet) in the southwestern portion of the basin as shown in Figure 24. To the north, the formation consists of complexly interbedded shales and sandstones, but to the south it consists of several thick, mappable sands and intervening shales. The formation dip is generally to the west, though, away from its onlap on the basement high to the east. It is truncated to the west by a basin-wide Paleocene-Eocene unconformity. Billions of cubic meters (hundreds of billions of cubic feet) of natural gas have been produced from the Mokelumne River Formation sands in the southern portion of the basin, indicating the suitability of these sands and their seals for sequestering a large volume of CO_2. As mentioned, these sands are also in proximity to several large CO_2 point sources.

The primary difference between the Sacramento Basin and the Illinois Basin relative with respect to the study of brine displacement is the variety of intrabasin structures. The Mokelumne River Formation was partially to completely cut by erosion of submarine canyons, as shown on Figure 24. These canyons, or "gorges," were subsequently filled, typically with mudstone. Natural gas has been produced from a number of unconformity traps where Mokelumne River sands are truncated by the gorge fills. The gorge fills therefore somewhat segment the Mokelumne River sands within the Sacramento Basin.

The Sacramento Basin has also been extensively faulted and folded at a sub-basin scale relative to the Illinois Basin. Natural gas has been produced from both fold and fault traps in the Mokelumne River sands. Figure 25 shows an example of this faulting in a natural gas field in the basin (CDOG 1982). Analysis of these faults indicates their development has been complex. They appear to have both growth and tectonic origins (Johnson 1990). They were extensional during deposition, but were reactivated in compression since the Miocene (Weber-Band 1998). It is likely that in addition to the faults shown on Figure 25, there are many smaller faults as well.

The sub-basin structures in the Sacramento Basin may cause different brine displacement behavior than in the Illinois Basin. Specifically, the intra-basin unconformities and faults may somewhat compartmentalize the formation. Alternatively, these structures may introduce flow barriers and anisotropies that direct flow along certain paths. For instance, the faults in the basin tend to strike north by northwest, therefore it may be that brine will be displaced preferentially in this direction. These questions motivate study of potential brine displacement the Sacramento Basin.

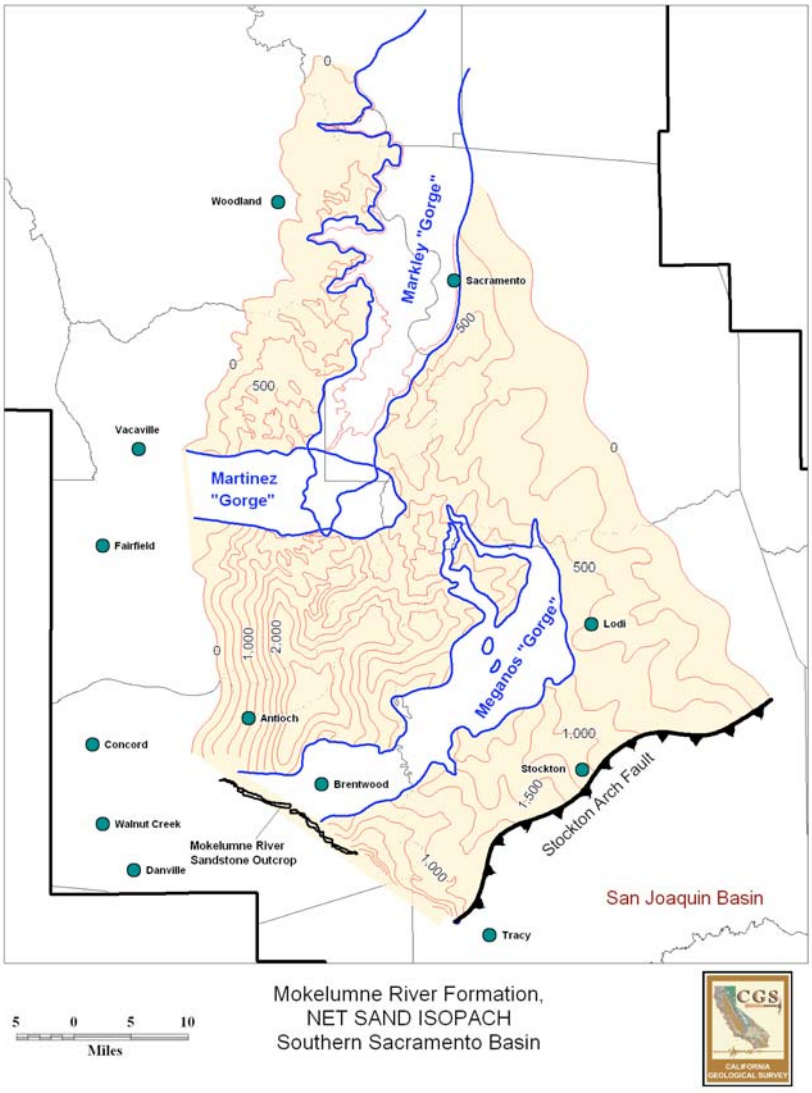

Figure 24. Contour map of the thickness of the Mokelumne River Formation (in feet) (Clinkenbeard 2007).

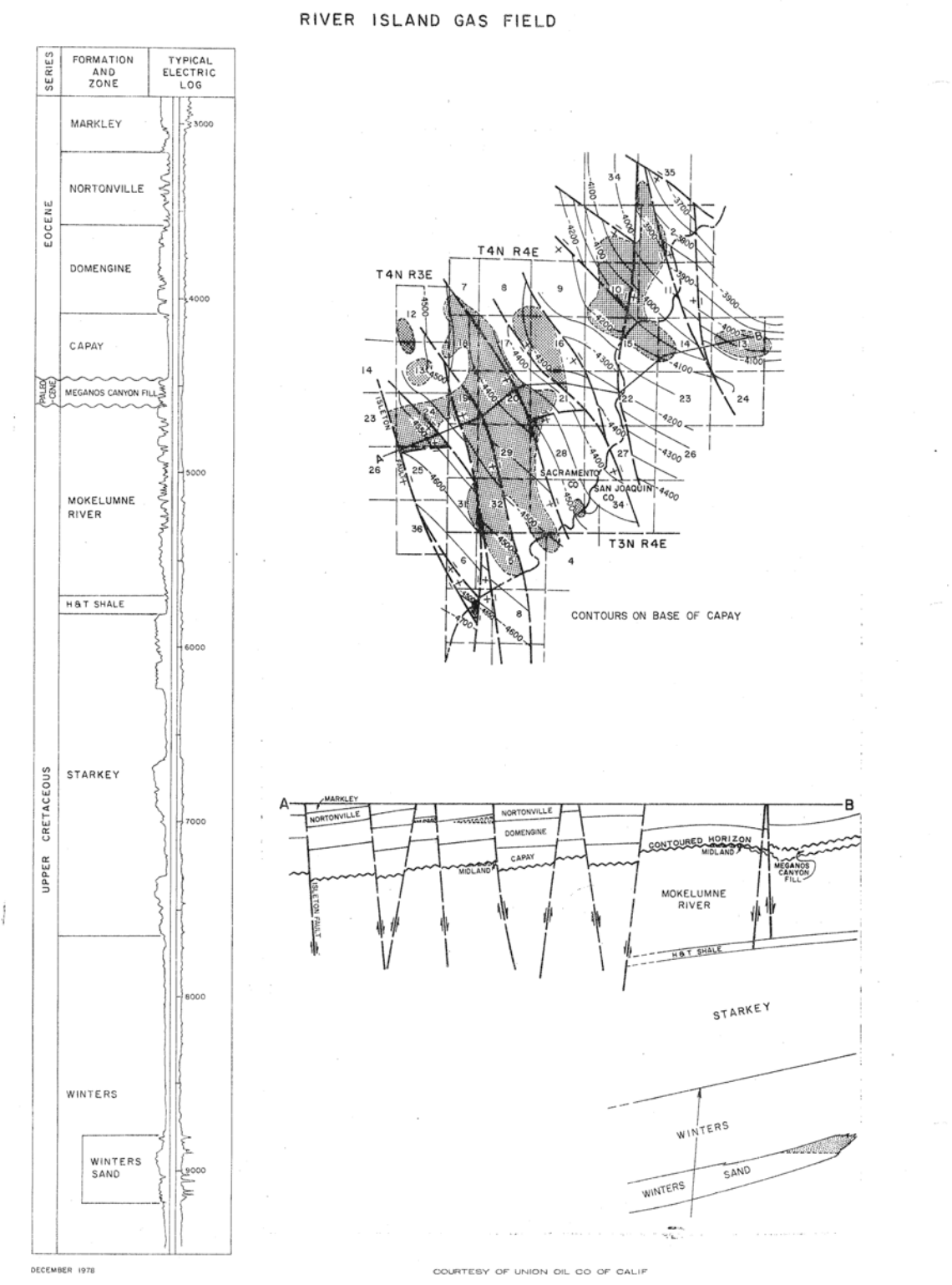

Figure 25. Example of faulting of the Mokelumne River Formation (CDOG 1982).

5.2.2. Parallelized Version of TOUGH2/ECO2N

As an important prerequisite for the computationally extensive basin-scale simulation studies envisioned in this research, the multi-phase simulator TOUGH2-ECO2N for CO_2 migration in brine aquifers at super- and subcritical conditions (Pruess, 2005) was adopted to run on a massively parallel computer cluster (Zhang et al., 2007). This new development, named TOUGH2-MP, makes possible the efficient simulation of CO_2 injection and brine migration in very large model domains. The simulator was applied to a basin-scale example study investigating CO_2 injection and brine migration. A three-dimensional geologic model of the stratigraphy was discretized with one million grid blocks. Using TOUGH2-MP on a 10-node Linux cluster, a transient non-isothermal multi-phase simulation run of CO_2 and brine migration with this discretization scheme was performed in less than a day.

6. Summary and Conclusions

Through numerical modeling of idealized subsurface formations, we have evaluated the possible impact of industrial-scale CO_2 injection on regional multilayered groundwater systems. The stored CO_2 replaces large volumes of native brine, which may cause considerable pressure perturbation and brine migration in the deep saline formations. If hydraulically communicating, either directly via updipping formations or through interlayer pathways such as faults or imperfect seals, these perturbations may impact shallow groundwater or even surface water resources used for domestic or commercial water supply. Possible environmental concerns include pressure and water table changes, changes in discharge and recharge zones, as well as changes in water quality. In compartmentalized formations, issues related to large-scale pressure buildup and brine displacement may also cause storage capacity problems, because significant pressure buildup can be produced. To address these issues, a three-year research program was initiated in October 2006, the first part of which is summarized in this report.

To date, systematic modeling studies have been conducted for two basic CO_2 injection scenarios. In Section 3, we have evaluated the pressure buildup and storage capacity in compartmentalized multilayer formations (closed and semi-closed systems), via detailed numerical simulations as well as approximate analytical solutions. Storage capacity in such formations is found to be generally much smaller than in open systems, because geomechanical damage due to overpressure needs to be avoided. In Section 4, we have simulated the pressure buildup and brine migration patterns in large laterally open systems, and have analyzed their respective regions of influence. For the conditions evaluated in this study, considerable pressure buildup was observed 100 km away from the injection zone, while the brine transport velocity and migration distance was less significant. Large-scale pressure changes appear to be of more concern to groundwater resources than changes in water quality due to, e.g., migration of saline waters into freshwater bodies. See summaries in Sections 3.6 and 4.4.

Our results demonstrate clearly the importance of evaluating the hydrologic perturbations generated by CO_2 storage. Any site assessment should consider the constraints imposed by pressure perturbation and brine displacement, either to avoid shallow-water impacts in open systems or to account for pressure constraints in closed systems. While the key properties of multilayered groundwater systems have been varied in a sensitivity study, which has enabled us to draw the above general conclusions, certain model simplifications and parameter choices may be inadequate at given storage sites. Thus, the systematic simulations conducted here should lead into site-specific modeling of CO_2 storage candidate sites, representing the local hydrogeological conditions. Two site-specific modeling studies of likely candidate sites for CO_2 storage, probably in the Illinois Basin and the California Central Valley, will be conducted in a future project phase (Section 5).

One interesting finding was the importance of seal permeability on pressure buildup and brine displacement behavior in the storage formation, in both closed and open systems. Seals that are suitable for long-term trapping of CO_2 may allow for considerable brine leakage out of the formation vertically upward and downward. As a result, the pressure buildup in the storage formation can be strongly reduced compared to a perfect seal with zero or close-to-zero permeability. It is thus important to fully understand the multilayer characteristics of a storage site when the large-scale brine displacement resulting from CO_2 injection, and the possible environmental impacts on USDWs, are to be investigated.

7. References

Bachu, S., W.D. Gunter, and E.H. Perkins, 1994. Aquifer disposal of CO2: hydrodynamic and mineral trapping, Energy Convers. Mgmt. 35(4), 269-279.

CDOG, 1982. California Oil and Gas Fields, Volume III: Northern California, Fourth Edition. California Division of Oil and Gas.

Clinkenbeard, 2007. Personal communication.

DOE (U.S. Department of Energy), 2007. Methodology for development of carbon sequestration capacity estimates, Appendix A in Carbon Sequestration Atlas of the United States and Canada, March 2007, National Energy Technology Laboratory, Pittsburgh, PA.

Domenico P.A., and F.W. Schwartz, 1998. Physical and Chemical Hydrogeology, 2nd edition, John Wiley & Sons, Inc. New York.

EPA (U.S. Environmental Protection Agency), 1994. Determination of maximum injection pressure for Class I wells, United States Environmental Protection Agency Region 5—underground injection control section regional guidance #7. EPA, Washington DC.

Fjar, E., R.M. Holt, P. Horsrud, and A.M. Raaen, 1991. Petroleum Related Rock Mechanics. Elsevier, Amsterdam.

Harris, 2006. Seismic monitoring of CO_2 sequestration, GCEP Technical Report, Stanford University, Palo Alto, CA.

Hart, D.J., 2000. Laboratory measurements of poroelastic constants and flow parameters and some associated phenomena, Ph.D. Thesis, University of Wisconsin-Madison, Madison, WI.

Hart, D.J., K.R. Bradbury, and D.T. Feinstein, 2006. The vertical hydraulic conductivity of an aquitard at two spatial scales, Ground Water, 44(2), 201–211.

Hildenbrand, A., S Schlömer, B. M Krooss, 2002. Gas breakthrough experiments on fine-grained sedimentary rocks, Geofluids, 2(1), 3-23.

Hildenbrand, A., Krooss, B.M., and S. Schlomer, 2003. N2 and CO2 gas breakthrough experiments on fine-grained sediments, In Poromechanics II, Proceedings of the Second Biot Conferences on Poromechanics, Grenoble, Eds. by J.L. Auriault, P. Royer, C. Geindreau, and J. F. Bloch, Aa Balkema.

Hovorka, S.D., C. Doughty, P.R. Knox, C.T. Green, K. Pruess, and S.M. Benson, 2001. Evaluation of brine-bearing sands of the Frio formation, upper Texas gulf coast for geological sequestration of CO_2. First National Conference on Carbon Sequestration, Washington, DC. 14–17 May, 2001. National Energy Technology Laboratory, Pittsburgh, PA.

Johnson, D.S., Rio Vista field-USA, Sacramento basin, Calif., in Foster, N.H., and Beaumont, E.A., eds., *Atlas of oil and gas fields, Structural Traps III*, AAPG Treatise of Petroleum Geology, Atlas of Oil and Gas Fields, Tulsa, Oklahoma, U.S.A., 1990.

Li, S., M. Dong, Z. Li, S. Huang, H. Qing and E. Nickel, 2005, Gas breakthrough pressure for hydrocarbon reservoir seal rocks: implications for the security of long-term CO2 storage in the Weyburn field, Geofluids, 5(4), 326-334.

Magoon, L.B. and C.V. Valin, 1995. 1995 National Oil and Gas Assessment: Sacramento Basin Province (009). United States Geological Survey.

Magoon, L.B. and Valin, Z.C., 1995, Sacramento Basin Province (009), *in,* Gautier, D. L., Dolton,G.L., Takahashi, K.I., and Varnes, eds., 1995 National assessment of United States oil and gas resources - results, methodology, and supporting data: U.S. Geological Survey Digital Data Series DDS-30, Release 2, one CD-ROM.

MGSC, 2005. An assessment of geological carbon sequestration options in the Illinois basin, Midwest Geologic Sequestration Consortium, Final Report.

MRCSP, 2005. Phase I Final Report, Midwest Regional Carbon Sequestration Partnership.

Muggeridge, A., Y. Abacioglu, W. England, and C. Smalley, 2004. Dissipation of anomalous pressures in the subsurface, Journal of Geophysical Research, 109, B11104, doi:10.1029/2003JB002922.

Neuzil, C.E., 1994. How permeable are clays and shales? Water Resour. Res., 30(2), 145–150.

Neuzil, C.E., 1995. Abnormal pressures as hydrodynamic phenomena, American Journal of Science, 295, 742–786.

Neuzil, C.E., 2003. Hydromechanical coupling in geologic processes, Hydrogeology J., 11, 41–83, DOI:10.1007/s10040-002-0230-8.

Nicot, J.-P., S. D. Hovorka, S. Lakshminarasimhan, 2006. Impact of carbon storage on shallow groundwater and pressure-controlled regional capacity for brine aquifers, Abstract in American Geophysical Union Fall Meeting, San Francisco, California, December 12.

Pruess, K, 2005. ECO2N: A TOUGH2 fluid property module for mixtures of water, NaCl, and CO_2, LBNL-57952, Lawrence Berkeley National Laboratory, Berkeley, CA.

Pruess, K., and J. Garcia, 2002. Multiphase flow dynamics during CO_2 disposal into saline aquifers, Environmental Geology, 42, 282–295.

Pruess, K., C. Oldenburg, G. Moridis, 1999. TOUGH2 User's Guide, Report LBNL-43134, Lawrence Berkeley National Laboratory, Berkeley, CA.

Puckette, J., and Al-Shaieb, Z., 2003. Naturally underpressured reservoirs: applying the compartment concept to the safe disposal of liquid waste, search and discovery article 40071, online adaptation of presentation at American Association of Petroleum Geologists, southwest section meeting, Fort Worth, TX, March, 2003 (www.southwestsection.org).

Rutqvist, J., and C.-F. Tsang, 2002. A study of caprock hydromechanical changes associated with CO_2-injection into a brine formation, Environmental Geology, 42, 296–305.

Rutqvist, J., J. Birkholzer, F. Cappa, and C.-F. Tsang, 2007a. Estimating maximum sustainable injection pressure during geological sequestration of CO_2 using coupled fluid flow and geomechanical fault-slip analysis, Energy Convers. Mgmt. 48, 1798–1807.

Rutqvist, J., J.T. Birkholzer, C.-F. Tsang, 2007b, Coupled reservoir-geomechanical analysis of the potential for tensile and shear failure associated with CO2 injection in multilayered reservoir-caprock systems, Int. J. Rock Mech. Mining Sci., doi:10.1016/j.ijrmms.2007.04.006.

USGS, Land subsidence in the United States, 1999. U.S. Geological Survey Circular 1182, Reston, Virginia, 1999.

van Genuchten, M.T., 1980. A closed form equation for predicting the hydraulic conductivity of unsaturated soils. Soil Sci. Soc. Am. J., 44, 892–898.

Weber-Band, J., Neotectonics of the Sacramento-San Joaquin Delta area, east-central Coast Ranges, California, University of California, Berkeley, doctoral thesis, 216 p., 1998.

WESTCARB, 2005. An overview of geologic sequestration potential in California, West Coast Regional Carbon Sequestration Partnership, Final Report.

Zhang, K., C. Doughty, Y.-S. Wu, K. Pruess, 2007. Efficient parallel simulation of CO2 geologic sequestration in saline aquifers, Proceedings SPE Reservoir Simulation Symposium, Houston, TX, February 2007.

8. Project Publications to Date

Birkholzer, J.T., Q. Zhou, C.-F. Tsang, J. Rutqvist, in preparation. Brine displacement due to large-scale CO_2 storage in saline formations: understanding the role of seal permeability, submitted to TBD.

Tsang, C.-F., Birkholzer, J.T., Q. Zhou, 2007. Pressure propagation and brine displacement in CO_2 storage formations: the role of sealing units, Abstract submitted to AGU Fall Meeting 2007, San Francisco, CA, December 2007.

Zhou, Q., J. Birkholzer, J. Rutqvist, C.-F. Tsang, 2007a. Sensitivity study of CO_2 capacity in brine aquifers with closed boundaries: dependence on hydrogeologic properties, Abstract submitted to 6th Annual Conference on Carbon Capture and Sequestration, Pittsburgh, PA, May 2007.

Zhou, Q., Birkholzer, J.T., Tsang, C.-F., Rutqvist, J.,2007b. Quick Assessment of CO2 Storage Capacity in Pressure-Constrained Saline Aquifers with Different Hydrogeologic Properties, Abstract submitted to AGU Fall Meeting 2007, San Francisco, CA, December, 2007.

Zhou, Q., Birkholzer, J.T., Tsang, C.-F., Rutqvist, J., in review. A method for quick-assessment of CO_2 storage capacity in pressure-constrained saline formations, submitted to Energy Conversion and Management.